GPCR-mediated calcium and cAMP signaling determines psychosocial stress susceptibility and resiliency

AUTHOR(S):

Inaba, Hiromichi; Li, Haiyan; Kawatake-Kuno, Ayako; Dewa, Ken-ichi; Nagai, Jun; Oishi, Naoya; Murai, Toshiya; Uchida, Shusaku

CITATION:

Inaba, Hiromichi ...[et al]. GPCR-mediated calcium and cAMP signaling determines psychosocial stress susceptibility and resiliency. Science Advances 2023, 9(14): eade5397.

ISSUE DATE:

2023-04

URL:

http://hdl.handle.net/2433/281568

SCIENCE ADVANCES | RESEARCH ARTICLE

NEUROSCIENCE

GPCR-mediated calcium and cAMP signaling determines psychosocial stress susceptibility and resiliency

Hiromichi Inaba[1,2], Haiyan Li[1]†, Ayako Kawatake-Kuno[1]†, Ken-ichi Dewa[3], Jun Nagai[3], Naoya Oishi[1], Toshiya Murai[1,2], Shusaku Uchida[1]*

Chronic stress increases the risk of developing psychiatric disorders, including mood and anxiety disorders. Although behavioral responses to repeated stress vary across individuals, the underlying mechanisms remain unclear. Here, we perform a genome-wide transcriptome analysis of an animal model of depression and patients with clinical depression and report that dysfunction of the Fos-mediated transcription network in the anterior cingulate cortex (ACC) confers a stress-induced social interaction deficit. Critically, CRISPR-Cas9–mediated ACC Fos knockdown causes social interaction deficits under stressful situation. Moreover, two classical second messenger pathways, calcium and cyclic AMP, in the ACC during stress differentially modulate Fos expression and regulate stress-induced changes in social behaviors. Our findings highlight a behaviorally relevant mechanism for the regulation of calcium- and cAMP-mediated Fos expression that has potential as a therapeutic target for psychiatric disorders related to stressful environments.

INTRODUCTION

Major depressive disorder (MDD) is a highly prevalent disorder, and its core symptoms include depressed mood, loss of interest or pleasure, suicidal thoughts, and lack of hope or motivation (*1*). Genetic epidemiological studies estimated the heritability of MDD at 37%, which is relatively low compared to that of schizophrenia and bipolar disorder (*2*), suggesting that factors other than genetic factors also contribute to the risk of depression. While genetic factors are important, stressful life events are also known to be associated with the etiology of this complex psychiatric disorder (*3*–*5*). Therefore, the current working hypothesis for the etiology of depression is that highly complex genetic (G) differences and environmental (E) factors work together (GxE interaction) to determine resilience and susceptibility to MDD (*5*–*7*).

Organisms must overcome adverse stressful experiences to survive, and the brain is the central organ that reacts and adapts to psychosocial stress. Successful adaptation to chronic stress is a dynamic process that is dependent on the attributes of the stress exposure, such as severity, modality, and duration (*8*, *9*). Stress "habituation" is presumed to be an important adaptive response to repeated challenges that allows an organism to a homeostatic state, promoting stress resilience. However, when stress exposure becomes chronic and severe for an individual, the stress response becomes maladaptive and results in detrimental effects, leading to pathological conditions (*8*–*11*).

Single strains of rodents are often used to establish an animal model of human diseases, yet the conclusions from such experiments are predicated on the assumption that they can be generalized to humans, which presupposes that they can at least be generalized to other inbred mouse strains (*12*). Different inbred strains of mice exhibit substantial differences in anxiety, stress reactivity, and drug responsiveness, and they can thus be used as animal models for investigating the influence of GxE factors on brain functions and behaviors (*13*–*19*). Among inbred mouse strains, we and others have demonstrated that the C57BL/6J (B6) strain shows stress habituation (i.e., a reduced stress response) to repeated stress exposure, whereas the BALB/c (BALB) strain lacks stress habituation to the same stressor and eventually exhibits depression-like behaviors (*13*–*15*). Thus, BALB mice are considered a stress-vulnerable strain, and comparing the stress responses of BALB and B6 mice allows us to decipher how GxE interactions shape adaptive and maladaptive responses at the molecular and cellular levels and to better understand the pathogenic mechanisms underlying depression, with potential for clinical translation.

Here, we aim to determine the molecular and cellular processes responsible for individual differences in psychosocial stress habituation and stress susceptibility. We applied brain-wide Fos mapping to obtain a comprehensive view of stress-activated/inhibited brain regions in mice exposed to social defeat stress (SDS) and identified the anterior cingulate cortex (ACC) as a key brain region involved in stress-induced social interaction deficit. We compared genome-wide gene expression in the ACC between susceptible mice and patients with major depression. This translational approach identified Fos as a crucial molecule associated with stress-elicited neuronal adaptation and social interaction behavior. Moreover, we report that G protein–coupled receptor (GPCR)–mediated calcium signaling and adenosine 3′,5′-monophosphate (cAMP) signaling during stress differentially modulate Fos expression and accordingly determine behavioral responses to stress. Thus, our findings highlight the distinct role of intracellular signaling pathways modulating *c-fos* expression in determining whether repeated stress facilitates or dampens stress resilience.

[1]SK Project, Medical Innovation Center, Kyoto University Graduate School of Medicine, 53 Shogoin-Kawahara-cho, Sakyo-ku, Kyoto 606-8507, Japan. [2]Department of Psychiatry, Kyoto University Graduate School of Medicine, 54 Shogoin-Kawahara-cho, Sakyo-ku, Kyoto 606-8507, Japan. [3]Laboratory for Glia-Neuron Circuit Dynamics, RIKEN Center for Brain Science, 2-1 Hirosawa, Wako, Saitama 351-0198, Japan.
*Corresponding author. Email: uchida.shusaku.3n@kyoto-u.ac.jp
†These authors contributed equally to this work.

RESULTS

Different mouse strains were used to test stress resilience and susceptibility

We first assessed behavioral differences following stress exposure in the context of a GxE model using two contrasting mouse strains, BALB, a highly stress-reactive strain, and B6, which is considered a less emotive strain (*13*, *14*, *18*). We subjected BALB and B6 mice to subchronic, mild SDS (smSDS; a 5-min SDS session/day for 5 days) (*13*) and assessed their social behaviors and anhedonia using the social interaction test (SIT) and sucrose preference test (SPT), respectively (Fig. 1A) (*13*, *14*, *20*). We found that BALB mice subjected to smSDS exhibited a significantly shorter social interaction time (Fig. 1B), a significant increase in the time spent in corner areas (Fig. 1C) in the SIT and a significant decrease in sucrose preference in the SPT (Fig. 1D), whereas B6 mice did not show these behavioral abnormalities following exposure to the same stressor (Fig. 1, B to D). These results suggest that BALB and B6 mice are smSDS-susceptible and smSDS-resilient strains, respectively. We also performed a tail suspension test (TST), which is used to evaluate rodents' motivation for escape behavior (*21*), and did not observe a significant difference in the immobility time between nonstressed and smSDS-exposed BALB mice (fig. S1, A and B).

We further analyzed the correlations of behavioral parameters from BALB mice subjected to 5 days of smSDS. We did not observe a significant correlation between the time spent in interaction zone of the SIT and the sucrose preference of the SPT (fig. S2), suggesting distinct mechanisms of behaviors in the SIT and SPT.

Brain-wide Fos mapping was mapped in stress-susceptible mice

We systematically mapped steady-state neuronal activity in BALB mice by performing immunohistochemistry for Fos, a marker of neuronal activity, to identify brain areas involved in the stress-susceptible phenotypes of BALB mice. Mice were euthanized 4 days after the last smSDS session (i.e., baseline Fos expression) along with nonstressed mice, and the number of Fos-positive cells in the ACC was quantified (Fig. 1E). We observed significantly

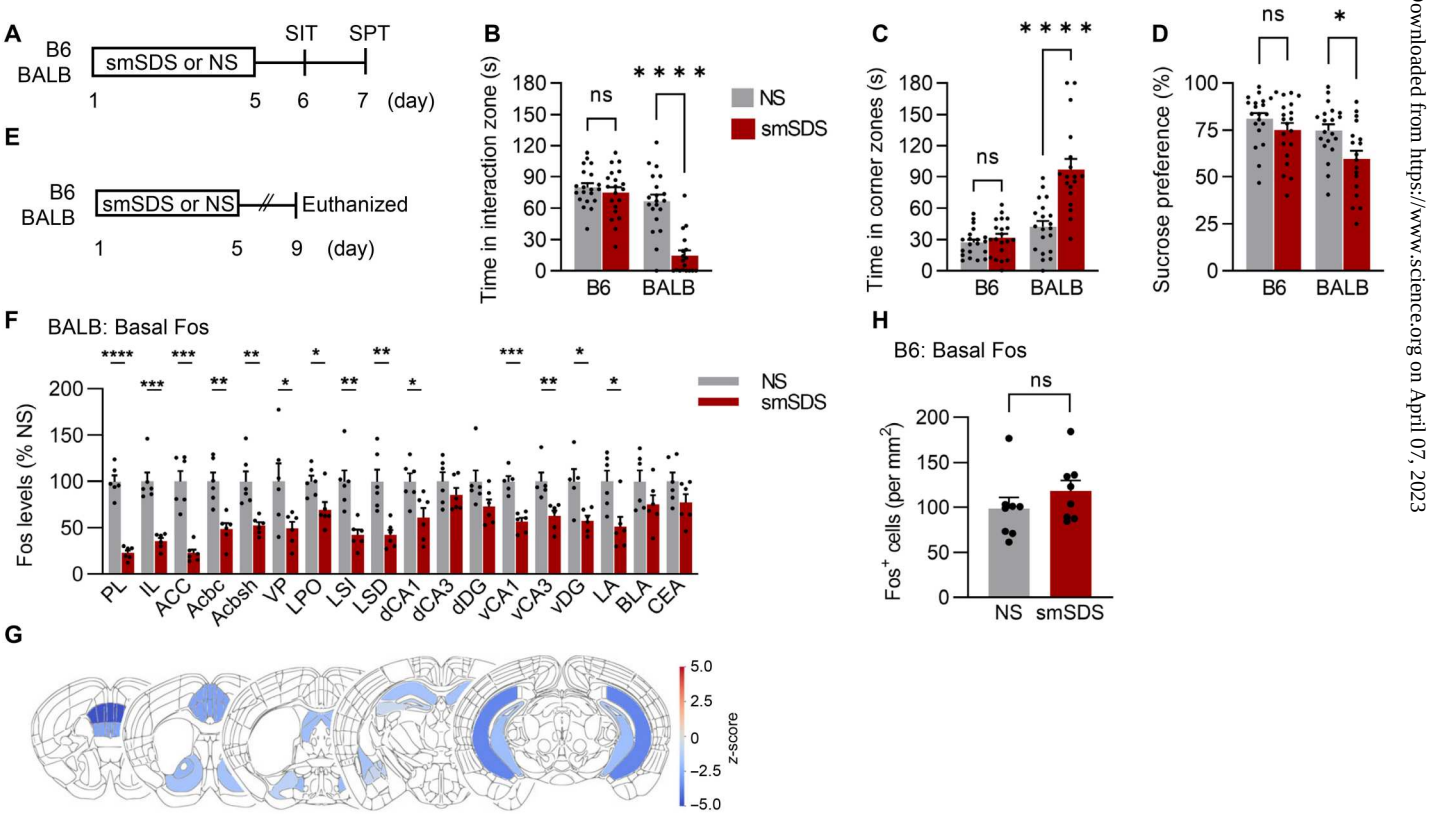

Fig. 1. Behavioral characterization and brain-wide Fos mapping of stress-susceptible and stress-resilient strains of mice. (**A**) The experimental design for behavioral testing. (**B** and **C**) Effects of 5 days of smSDS exposure on the time spent in the interaction zone (B) and the time spent in the corner zones (C) of the SIT [interaction zone: two-way analysis of variance (ANOVA), strain × stress, $F_{1,74} = 19.88$, $P < 0.0001$; post hoc test, nonstress (NS)–BALB versus smSDS-BALB, $P < 0.0001$; corner zones: two-way ANOVA, strain × stress, $F_{1,74} = 18.17$, $P < 0.001$; post hoc test, NS-BALB versus smSDS-BALB, $P < 0.0001$] in B6 and BALB mice. $n = 18$ to 20 per group. (**D**) Effect of 5 days of smSDS exposure on sucrose preference measured using the SPT in B6 and BALB mice (two-way ANOVA, strain, $F_{1,74} = 9.031$, $P < 0.01$, stress, $F_{1,74} = 8.791$, $P < 0.01$; post hoc test, NS-BALB versus smSDS-BALB, $P < 0.05$). $n = 18$ to 20 per group. (**E**) The experimental design for quantifying baseline Fos expression. B6 and BALB mice were subjected to 5 days of smSDS or NS, and mice were euthanized for Fos staining 4 days later. (**F**) Quantification of Fos immunostaining in multiple brain regions of BALB mice 96 hours after the last smSDS session and in NS controls. $n = 6$ per group. (**G**) Schematic depicting the brain-wide Fos analysis of BALB mice subjected to 5 days of smSDS compared with NS controls. Fos immunoreactivity was unchanged (light gray), increased (red), or decreased (blue). (**H**) Quantification of Fos immunostaining in the ACC of B6 mice 96 hours after the last smSDS session and in NS controls. $n = 8$ per group. ****$P < 0.0001$, ***$P < 0.001$, **$P < 0.01$, *$P < 0.05$. Bar graphs show the means ± SEM. ns, not significant.

lower Fos immunoreactivity in many brain regions of BALB mice subjected to smSDS than in nonstressed mice (Fig. 1, F and G). Among these brain areas, the reduction in Fos levels in the medial prefrontal cortex (mPFC), including the prelimbic, infralimbic, and ACC areas, was clearly affected by 5 days of smSDS exposure (Fig. 1F). Exposure to smSDS reduced Fos levels by approximately 77.2% in the ACC of BALB mice. In contrast, baseline Fos levels in the ACC of B6 mice subjected to smSDS were comparable to those in nonstressed controls (Fig. 1H). These data suggest that the smSDS-induced reduction in baseline Fos expression in the ACC of BALB mice may be associated with the development of stress-induced depression-like behaviors.

There are distinct Fos induction patterns during the response to social stimuli in B6 and BALB mice

Successful stress habituation is defined by a decreasing central response to stressors, as measured by Fos expression in the brain (*11*, *22*). We further examined whether neuronal activity in response to social stress exposure was changed during a 5-day smSDS episode. For this experiment, BALB mice were subjected to 5 days of smSDS or nonstress and exposed to an unfamiliar CD1 mouse (as a social stimuli) or remained in their home cage 4 days later and then perfused 90 min after the social stimuli for Fos staining (Fig. 2A). We quantified Fos protein expression in 18 brain regions and constructed a brain-wide Fos map for social stimuli-induced neuronal activation in BALB mice (Fig. 2, B to G). We detected social stimuli-induced Fos expression in the lateral preoptic area (LPO), dorsal part of lateral septal nucleus (LSD), dorsal region of Ammon's horn 3 (dCA3), ventral region of Ammon's horn 1 (vCA1), ventral region of Ammon's horn 3 (vCA3), lateral amygdala (LA), and basolateral amygdala (BLA), but not in the ACC, of nonstressed BALB mice (Fig. 2, C and E), whereas BALB mice subjected to smSDS showed significantly greater Fos expression in the 18 brain regions examined in this study upon exposure to social stimuli (Fig. 2, D and F). In contrast to BALB mice, nonstressed B6 mice showed significantly greater Fos expression in the ACC upon social stimulus exposure, and this increase in Fos expression was significantly decreased in mice exposed to 5 days of smSDS (Fig. 2H). These results indicate that compared to nonstressed mice, the smSDS-susceptible BALB strain exhibited sensitized Fos responses when exposed to social stimuli (Fig. 2, G and I) and that the smSDS-resilient B6 strain exhibited a desensitized response upon social stimulus exposure (Fig. 2I).

On the basis of these findings, we hypothesized that the sensitization of the ACC neuronal response to repeated stress exposure reduces baseline Fos expression and induces depression-related behaviors in BALB mice, whereas successful stress habituation induced by the same stressor prevents the reduction in baseline Fos expression and aberrant behaviors in B6 mice. We first aimed to investigate the role of ACC in smSDS-induced behavioral changes to test this hypothesis. Second, in addition to the role of Fos as an activity marker, its inherent roles in plasticity and behavior remain unclear (*23*). We therefore examined the role of baseline Fos expression in stress susceptibility and resilience. Third, we used multiple genetic tools to clarify how the ACC neuronal response to daily stressful events (i.e., sensitization and desensitization) influences baseline Fos levels and subsequent behavioral changes.

Ablation of ACC glutamatergic neurons leads to strain-dependent changes in stress vulnerability and behaviors

The ACC is suggested to be involved in multiple brain functions, including mood, anxiety, social behavior, memory, and antidepressant functions (*17*, *24*–*28*). As a method to investigate whether the activity of ACC neurons is required to regulate a subset of depression-related behaviors following repeated stress exposure, we performed a loss-of-function study that used a genetic approach to selectively ablate ACC neurons in adult mice. In this experiment, we injected a Cre-dependent adeno-associated virus (AAV) encoding a modified pro-caspase 3 and Tobacco Etch Virus (TEV) protease (AAV-EF1a-FLEX-taCasp3-TEVp) (*29*) into the ACC of vGlut-Cre mice (B6 genetic background) to selectively target ACC glutamatergic neurons (Fig. 3, A and B). Control mice were injected with a Cre-dependent tdTomato construct (AAV-EF1a-FLEX-tdTomato). Four weeks after the AAV injection, the mice were subjected to 5 days of smSDS and then performed the SIT, SPT, and TST. We detected tdTomato expression in the ACC of control mice (Fig. 3C), and terminal deoxynucleotidyl transferase–mediated deoxyuridine triphosphate nick end labeling (TUNEL) staining confirmed increased apoptosis in vGlut-Cre mice expressing taCasp3-TEVp but not in control tdTomato mice (Fig. 3D). Behaviorally, mice lacking ACC glutamatergic neurons did not exhibit any behavioral abnormalities in the SIT, SPT, or TST under the nonstressed condition (Fig. 3, E to G). However, compared to nonstressed controls, mice with smSDS exposure and lacking ACC glutamatergic neurons spent significantly less time in the interaction zone in the SIT and exhibited a significantly greater immobility time in the TST but a normal sucrose preference in the SPT (Fig. 3, E to G). Thus, ACC glutamatergic neurons are required to regulate social interaction and motivated escape behaviors in B6 mice.

Because stressed BALB mice exhibited reduced social interactions and sucrose preference (Fig. 1), we next investigated whether the selective ablation of ACC glutamatergic neurons altered these depression-related behaviors in BALB mice. We injected BALB mice with AAV-Camk2a-Cre together with AAV-EF1a-FLEX-taCasp3-TEVp or AAV-EF1a-FLEX-tdTomato (Fig. 3, H to J). TUNEL staining revealed increased apoptosis in the ACC of mice expressing taCasp3-TEVp (Fig. 3K). We found that BALB mice lacking ACC glutamatergic neurons exhibited a significantly decreased time in the interaction zone in the SIT, a significantly greater immobility time in the TST, and a normal sucrose preference in the SPT when compared to those of the tdTomato-expressing control groups (Fig. 3, L to N). On the basis of these results, ablation of ACC glutamatergic neurons induces social interaction deficits and reduced motivated escape behaviors, but not sucrose preference, in BALB mice.

Genome-wide expression analyses of the ACC was performed in stress-susceptible mice

We performed RNA sequencing (RNA-seq) to compare genome-wide transcriptional changes in the ACC of stressed and nonstressed BALB mice and elucidate the molecular mechanism underlying smSDS-mediated depression-like behaviors (Fig. 4, A to D, and data S1). We found 290 differentially expressed genes (DEGs) that were up-regulated (150 genes) or down-regulated (140 genes) by smSDS exposure. To identify converging MDD-related transcriptional pathways in the ACC of BALB mice subjected to smSDS, we used publicly available RNA-seq data from the ACC of human

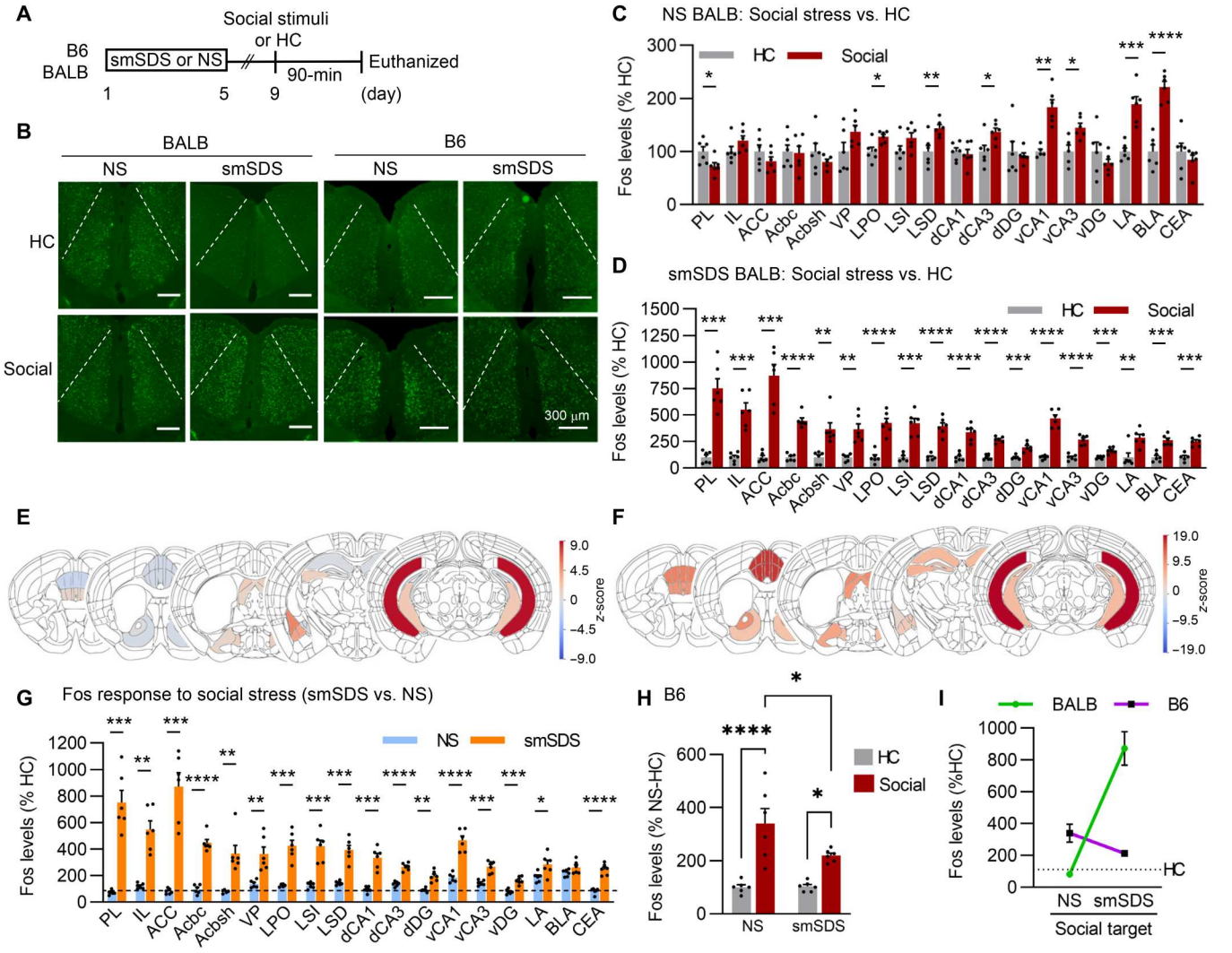

Fig. 2. Distinct Fos induction during the response to acute social stimuli in B6 and BALB mice. (**A**) The experimental design of Fos quantification for evaluating stress habituation. B6 and BALB mice were subjected to 5 days of smSDS or NS. The mice were then exposed to an unfamiliar CD1 mouse (social stimulus) through a perforated transparent divider or remained in their home cage and then were perfused 90 min after the social stressor exposure for Fos staining. (**B**) Representative coronal slices showing Fos expression in the ACC of BALB and B6 mice. Scale bars, 300 μm. (**C** and **D**) Quantification of Fos immunostaining in multiple brain regions of BALB mice subjected to NS (C) or 5 days of smSDS (D) 90 min after exposure to a social stimulus. $n = 6$ per group. (**E** and **F**) Schematic depicting the brain-wide Fos analysis of BALB mice subjected to NS (E) or 5 days of smSDS (F) in response to social stimulation compared with home cage (HC) controls. (**G**) A comparison of Fos induction upon exposure to a social target compared to the HC between NS and smSDS BALB mice. $n = 6$ per group. (**H**) Quantification of Fos immunostaining in the ACC of B6 mice subjected to NS or 5 days of smSDS after exposure to a social target (two-way ANOVA, stress × social interaction, $F_{1,20} = 4.528$, $P < 0.05$; post hoc test, NS-HC versus NS-social, $P < 0.0001$, smSDS-HC versus smSDS-social, $P < 0.05$, NS-social versus smSDS-social, $P < 0.05$). $n = 6$ per group. (**I**) A summary graph showing distinct Fos induction patterns between BALB and B6 mice [Fos quantification data from (G) and (H)]. ****$P < 0.0001$, ***$P < 0.001$, **$P < 0.01$, *$P < 0.05$. Bar graphs show the mean ± SEM.

MDD (*30*) and compared the transcriptional profiles from the mouse model with those from human MDD (Fig. 4B). Three genes (i.e., *Mmp16*, *Ccdc66*, and *Zfc3h1*) were commonly up-regulated, and seven genes (i.e., *c-fos*, *Nr4a1*, *Junb*, *Hapln4*, *Nefh*, *Dusp5*, and *Rpp38*) were commonly down-regulated in both the BALB model and humans with MDD. In addition, we analyzed 290 DEGs (150 up-regulated and 140 down-regulated genes) using Metascape (*31*). The results showed that the significantly enriched signaling pathways for the down-regulated DEGs included negative regulation of protein ubiquitination, antigen processing, and membrane depolarization (Fig. 4E), and the significantly enriched signaling pathways for the up-regulated DEGs included synapse organization, cell-cell adhesion molecules, and synapse assembly (Fig. 4F). Furthermore, protein-protein interaction (PPI) networks were constructed by Metascape for down-regulated DEGs (Fig. 4G) and up-regulated DEGs (Fig. 4H), and the functional modules of the PPI networks were filtered by MCODE. MCODE analysis demonstrated that the DEGs were grouped into four modules. Briefly, for the down-regulated DEGs (Fig. 4G), module 2 comprised three genes, namely, *Fos*, *Junb*, and *Mapk12*, and module 3 comprised three genes, namely, *Cry1*, *Per1*, and *Per2*. For the up-regulated DEGs (Fig. 4H), module 1 comprised eight genes, including

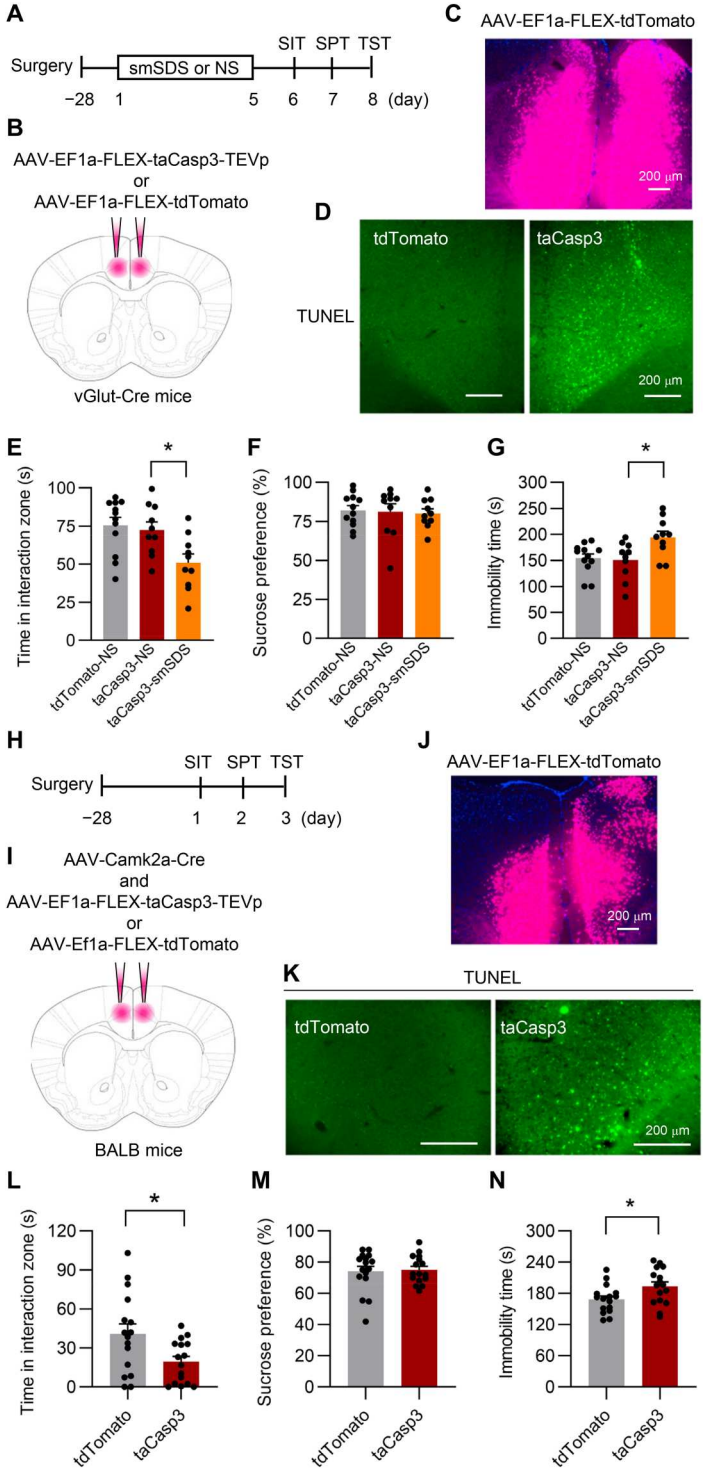

Fig. 3. Ablation of ACC glutamatergic neurons increases depression-related behaviors. (**A**) The experimental design for behavioral testing. (**B**) AAV microinjection into the ACC. (**C**) A representative image of injection of AAV-EF1a-FLEX-tdTomato into the ACC of vGlut-Cre mice. Scale bar, 200 μm. (**D**) Images of TUNEL staining in coronal sections of the ACC region of mice injected with AAV-EF1a-FLEX-tdTomato (left) or AAV-EF1a-FLEX-taCasp3-TEVp (right). Scale bars, 200 μm. (**E** to **G**) The time spent in the interaction zone of the SIT (E) (one-way ANOVA, $F_{2,29} = 6.075$, $P < 0.01$; post hoc test, taCasp3-NS versus taCasp3-smSDS, $P < 0.05$), sucrose preference in the SPT (F) (one-way ANOVA, $F_{2,29} = 0.07$, $P > 0.05$), and immobility time in the TST (G) (one-way ANOVA, $F_{2,29} = 5.236$, $P < 0.05$; post hoc test, taCasp3-NS versus taCasp3-smSDS, $P < 0.01$). $n = 10$ to 12 per group. (**H**) The experimental design for behavioral testing of BALB mice. (**I**) AAV microinjection into the ACC of BALB mice. (**J**) A representative image of injection of AAV-Camk2a-Cre and AAV-EF1a-FLEX-tdTomato into the ACC of BALB mice. Scale bar, 200 μm. (**K**) Images of TUNEL staining in coronal sections of the ACC region of BALB mice injected with AAV-Camk2a-Cre together with AAV-EF1a-FLEX-tdTomato (left) or AAV-EF1a-FLEX-taCasp3-TEVp (right). Scale bars, 200 μm. (**L** to **N**) Time spent in the interaction zone of the SIT (L) (Welch's test, $t_{22.79} = 2.448$, $P < 0.05$), sucrose preference in the SPT (M) (unpaired t test, $t_{30} = 0.2564$, $P > 0.05$), and immobility time in the TST (N) (unpaired t test, $t_{30} = 2.31$, $P < 0.05$). $n = 16$ per group. *$P < 0.05$. Bar graphs show the means ± SEM.

Cntn5, *Ncam2*, *Ptpn4*, and *Grid2*, and module 2 comprised seven genes, including *Kcna4*, *Kcna3*, and *Rps29*. It should be noted that TRRUST database analysis revealed *Cebpb*, *Fos*, *Clock*, and *Nfkb1* to be the main transcription factors regulating the hub genes (Fig. 4I).

We confirmed the expression of common DEGs between the mouse model and humans with MDD by performing quantitative polymerase chain reaction (qPCR) analyses of the different mouse tissue samples used to obtain the previous RNA-seq datasets shown in Fig. 4A. We found that the expression of *c-fos*, *Junb*, and *Nr4a1* in BALB mice subjected to smSDS was significantly lower than that in nonstressed BALB mice (Fig. 4J). The expression of *Mmp16* and *Zfc3h1* in BALB mice subjected to smSDS was significantly greater than that in nonstressed BALB mice. In contrast, we did

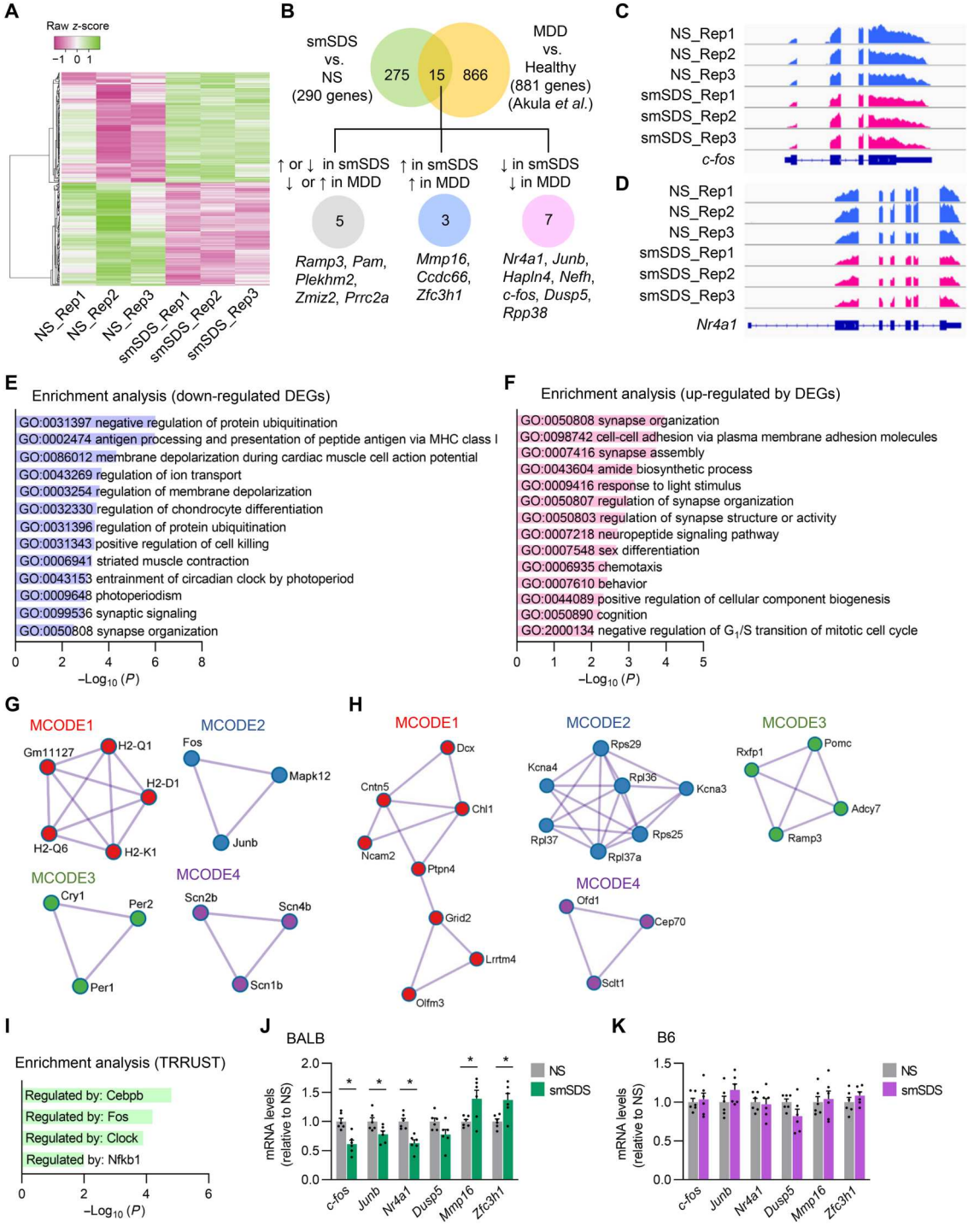

Fig. 4. RNA-seq reveals transcriptional alterations in the ACC of BALB mice subjected to smSDS that predict Fos as an upstream regulator. (**A**) Heatmap comparing gene expression patterns for the subchronic and smSDS versus NS groups. Samples were collected 48 hours after the last smSDS session ($n = 3$ per group). Rep, replicate. (**B**) Venn diagram depicting the overlapping genes between BALB mice subjected to smSDS and postmortem tissues from patients with major depression (*30*). (**C** and **D**) Sequencing tracks showing *c-fos* (C) and *Nr4a1* (D) genes modified by 5-day smSDS episodes. $n = 3$ mice per group. (**E** and **F**) Functional enrichment analysis of down-regulated (E) and up-regulated (F) genes after 5 days of smSDS exposure using Metascape. (**G** and **H**) Four MCODE complexes identified in Metascape for down-regulated (G) and up-regulated (H) genes after 5 days of smSDS exposure. DEGs were divided into four modules based on function, and protein-protein interaction (PPI) networks were constructed for the DEGs of each module. (**I**) Enrichment of transcriptional regulators of hub genes using the TRRUST database. (**J**) Quantitative polymerase chain reaction (qPCR) validation of the expression levels of six genes whose expression was altered in the ACC of stressed BALB mice and patients with major depression, as shown in (B) (multiple unpaired *t* test: *c-fos*, $q = 0.0005$; *Junb*, $q = 0.016$; *Nr4a1*, $q = 0.005$; *Mmp16*, $q = 0.005$; *Zfc3h1*, $q < 0.005$). $n = 6$ per group. (**K**) qPCR validation of the gene expression levels of six genes measured in (J) in the ACC of stressed B6 mice ($n = 6$ per group). $^*P < 0.05$. Bar graphs show the means ± SEM.

not find any significant alterations in the expression of these five genes in B6 mice subjected to smSDS compared to nonstressed B6 mice (Fig. 4K). Overall, these analyses of a mouse model and humans with MDD support our hypothesis that an aberrant Fos-mediated transcriptional network within the ACC might be involved in depression.

Fos function in ACC glutamatergic neurons is required for social behaviors under stressful challenges

As mentioned above, Fos is a well-studied immediate early gene product used as a marker of neuronal activation, whereas its role in brain function and behaviors is being investigated (*23*). We selectively knocked down Fos in ACC glutamatergic neurons by injecting an AAV vector expressing *Staphylococcus aureus* Cas9 (SaCas9) (*32*) under the control of the *Camk2a* promoter together with a single-guide RNA (sgRNA) targeting *c-fos* (sgFos) into adult B6 mice to induce conditional knockdown (CKD) of Fos in the ACC to provide a causal link between the decreased baseline Fos expression and increased stress susceptibility (Fig. 5, A and B). Control mice received AAVs expressing SaCas9 together with the scrambled sgRNA (sgControl). Immunohistochemistry revealed that this CRISPR/SaCas9-mediated genome-editing technique drastically reduced Fos expression in the ACC of Fos CKD mice (Fig. 5C). We then exposed Fos CKD mice to 5 days of smSDS and performed behavioral tests (Fig. 5A). We found that Fos CKD mice did not show any behavioral deficits in the SIT, SPT, or TST under nonstressed conditions (Fig. 5, D to H). Following smSDS exposure, however, Fos CKD mice spent significantly less time in the interaction zone (Fig. 5, D and E) but a normal amount of time in the corner zones of the SIT (Fig. 5F) compared to nonstressed Fos CKD mice. Sucrose preference in the SPT and immobility time in the TST of Fos CKD mice were comparable to those of nonstressed Fos CKD mice (Fig. 5, G and H). These results suggest the crucial role of Fos function in ACC glutamatergic neurons in controlling social behavior under stressful conditions.

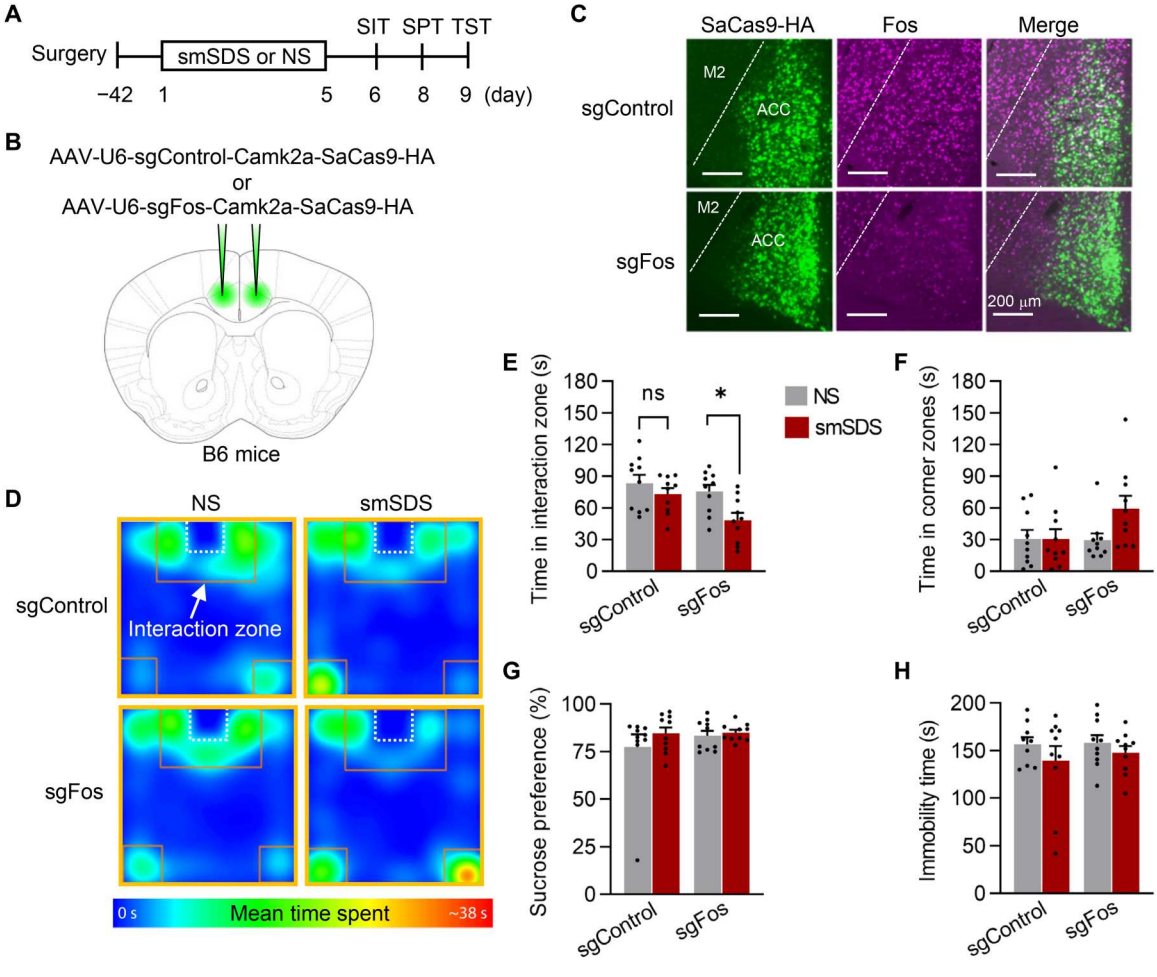

Fig. 5. Fos knockdown in ACC glutamatergic neurons induces strain-dependent differences in stress vulnerability and social behavior deficits. (**A**) The experimental design for behavioral testing. (**B**) AAV microinjection into the ACC. (**C**) Immunohistochemical staining confirms knockdown of the Fos protein in SaCas9-HA–expressing glutamatergic neurons of the ACC of B6 mice injected with AAV-U6-sgFos-Camk2a-SaCas9-HA. Scale bars, 100 μm. (**D** to **F**) Representative heatmaps (D), the time in the interaction zone (E) (two-way ANOVA, stress, $F_{1,36} = 7.539$, $P < 0.01$, sgRNA, $F_{1,36} = 5.854$, $P < 0.05$; post hoc test, NS-sgFos versus smSDS-sgFos, $P < 0.05$), and the time in the corner zones (F) in the SIT. $n = 10$ per group. (**G**) Sucrose preference in the SPT. $n = 10$ per group. (**H**) Immobility time in the TST. $n = 10$ per group. *$P < 0.05$. Bar graphs show the means ± SEM.

Chemogenetic activation of Gq-GPCR signaling in ACC glutamatergic neurons induces a social interaction deficit

Because ACC neurons in BALB mice subjected to 5 days of smSDS were sensitized when exposed to an acute social stressor but those of B6 mice were desensitized by the same stressor (Fig. 2I), we tested whether the repeated activation of ACC neurons is sufficient to induce depression-related behaviors. For this experiment, we mimicked the activation of ACC glutamatergic neurons in response to a psychosocial stressor using the chemogenetic tool Designer Receptor Exclusively Activated by Designer Drugs (DREADDs) (*33*). We used Gq-coupled receptor hM3Dq-DREADD, which induces neural activation via phospholipase C–dependent calcium signaling upon clozapine N-oxide (CNO) treatment (*34*). The AAV vector containing hM3Dq-DREADD (AAV-Syn-DIO-hM3Dq-mCherry) was injected into the ACC of vGlut-Cre mice (strain B6) to specifically express the chemogenetic neuromodulator hM3Dq on glutamatergic neurons in the ACC (Fig. 6A). We performed Fos immunohistochemistry 90 min after treatment with CNO or vehicle (Fig. 6B) to validate the efficacy of the DREADD system and found that CNO significantly increased the percentage of Fos induction in hM3Dq-mCherry–expressing glutamatergic neurons (Fig. 6, C and D). Then, the mice were systemically injected with CNO once per day for five consecutive days and subjected to the SIT and SPT (Fig. 6E). CNO-treated hM3Dq mice spent significantly less time in the interaction zone of the SIT (Fig. 6F) than vehicle-treated hM3Dq mice but exhibited a normal sucrose preference in the SPT (Fig. 6G).

We also tested whether BALB mice showed social deficits following repeated activation of ACC glutamatergic neurons. The ACC of BALB mice was injected with AAVs expressing hM3Dq-mCherry under the control of the *Camk2a* promoter (Fig. 6H), and 21 days later, we validated the efficacy of the DREADD system in this strain. We confirmed the successful induction of Fos expression in hM3Dq-mCherry–expressing glutamatergic neurons 90 min after treatment with CNO (Fig. 6, I to K). Then, the mice were systemically injected with CNO once per day for five consecutive days and tested in the SIT and SPT (Fig. 6L). Similar to B6 mice, BALB mice that expressed hM3Dq and were treated with CNO spent significantly less time in the interaction zone of the SIT (Fig. 6M) than vehicle-treated BALB mice expressing hM3Dq but exhibited a normal sucrose preference in the SPT (Fig. 6N). We next examined the effect of repeated activation of ACC glutamatergic neurons on baseline Fos expression (5 days after the last daily CNO treatment; Fig. 6L) and found that baseline Fos levels in the ACC were significantly lower in CNO-treated hM3Dq mice than in vehicle-treated hM3Dq mice (Fig. 6, O and P). Together, these results suggest that repeated Gq-GPCR activation in ACC glutamatergic neurons reduces baseline Fos levels and induces social interaction deficits, but not changes in sucrose preference.

Attenuation of Gq-GPCR signaling in ACC glutamatergic neurons during stress drives stress resilience

We next tested whether silencing Gq-GPCR signaling in ACC glutamatergic neurons during daily SDS exposure would be sufficient to block the expression of social interaction deficits following 5 days of smSDS exposure. For this experiment, we used inhibitory peptide from β-adrenergic receptor kinase 1 (iβARK), an inhibitory peptide containing the regulator of G-protein signaling homology domain of β-adrenergic receptor kinase 1, which selectively attenuates Gq-GPCR–evoked Ca^{2+} signaling (*35*). iβARK directly binds to $G\alpha_{q/11}$ subunits and thus sequesters them to block subsequent Gq-GPCR–induced intracellular calcium signaling cascades (*35*). BALB mice were injected with AAV-Camk2a-Cre together with either AAV-CAG-FLEX-iβARK-P2A-mCherry, AAV-CAG-FLEX-iβARK(D110A)-P2A-mCherry as an inactive control, or AAV-CAG-FLEX-mCherry as a blank control into the ACC (Fig. 7A). We first validated the efficacy of iβARK in our experiment and measured Fos expression as a marker of neuronal activation 90 min after the sixth SDS exposure in mice subjected to 5 days of smSDS (sensitized mice as shown in Fig. 2I) (Fig. 7B). Notably, iβARK mice showed significantly less Fos induction in response to the sixth SDS exposure than iβARK(D110A) or mCherry mice (Fig. 7, C and D), suggesting the successful stress habituation of iβARK mice. BALB mice subjected to 5 days of smSDS then performed the SIT and SPT (Fig. 7E), and we found that compared to iβARK(D110A) and mCherry mice, iβARK mice spent significantly more time in the interaction zone of the SIT (Fig. 7F) and exhibited a comparable sucrose preference in the SPT (Fig. 7G). We next quantified baseline Fos levels in the ACC of iβARK mice 72 hours after 5- days of smSDS exposure (Fig. 7H) and found that the number of Fos-positive cells in stressed iβARK mice was comparable to that in nonstressed mCherry mice, whereas mCherry and iβARK(D110A) mice subjected to 5 days of smSDS displayed a significantly lower Fos levels (Fig. 7, H and I). On the basis of these results, Gq-GPCR–mediated calcium signal attenuation in the ACC during stress prevents the repeated stress-induced reduction in baseline Fos levels and drives stress resilience.

Chemogenetic activation of Gi-GPCR signaling in ACC glutamatergic neurons during stress induces social interaction deficits

Because the attenuation of the Gq-GPCR signal in the ACC during smSDS drives stress resilience, we confirmed whether silencing the activity of ACC glutamatergic neurons during daily SDS exposure by stimulating Gi-GPCR signaling also effectively drives stress resilience. We achieved this goal using hM4Di-DREADD, which induces neuronal inhibition via cAMP-mediated signaling upon CNO treatment (*33*, *34*). The AAV vector containing the inhibitory Gi-coupled receptor hM4Dq (AAV-Syn-DIO-hM4Di-mCherry) was injected into the ACC of vGlut-Cre mice (strain B6) (Fig. 8A). We performed Fos immunohistochemistry to validate the efficacy of the inhibitory DREADD system and observed greater Fos expression in mCherry-positive glutamatergic neurons 90 min after SDS exposure, whereas this induction was blocked by pretreatment with CNO (30 min before SDS exposure) (fig. S3, A to C), suggesting successful inhibition of SDS-evoked ACC glutamatergic neuronal activity by hM4Di-DREADD. Then, we investigated behavioral outcomes after the specific inhibition of ACC glutamatergic neurons during the 5 days of smSDS exposure. The mice were systemically injected with CNO 30 min before SDS exposure during the 5 days of smSDS exposure and then subjected to the SIT and SPT (Fig. 8B). Unexpectedly, however, we found that smSDS-exposed mice treated with CNO during 5 days of smSDS spent significantly less time in the interaction zone (Fig. 8C) and more time in corner zones (Fig. 8D) in the SIT than CNO-treated nonstressed mice but exhibited a normal sucrose preference in the SPT (Fig. 8E).

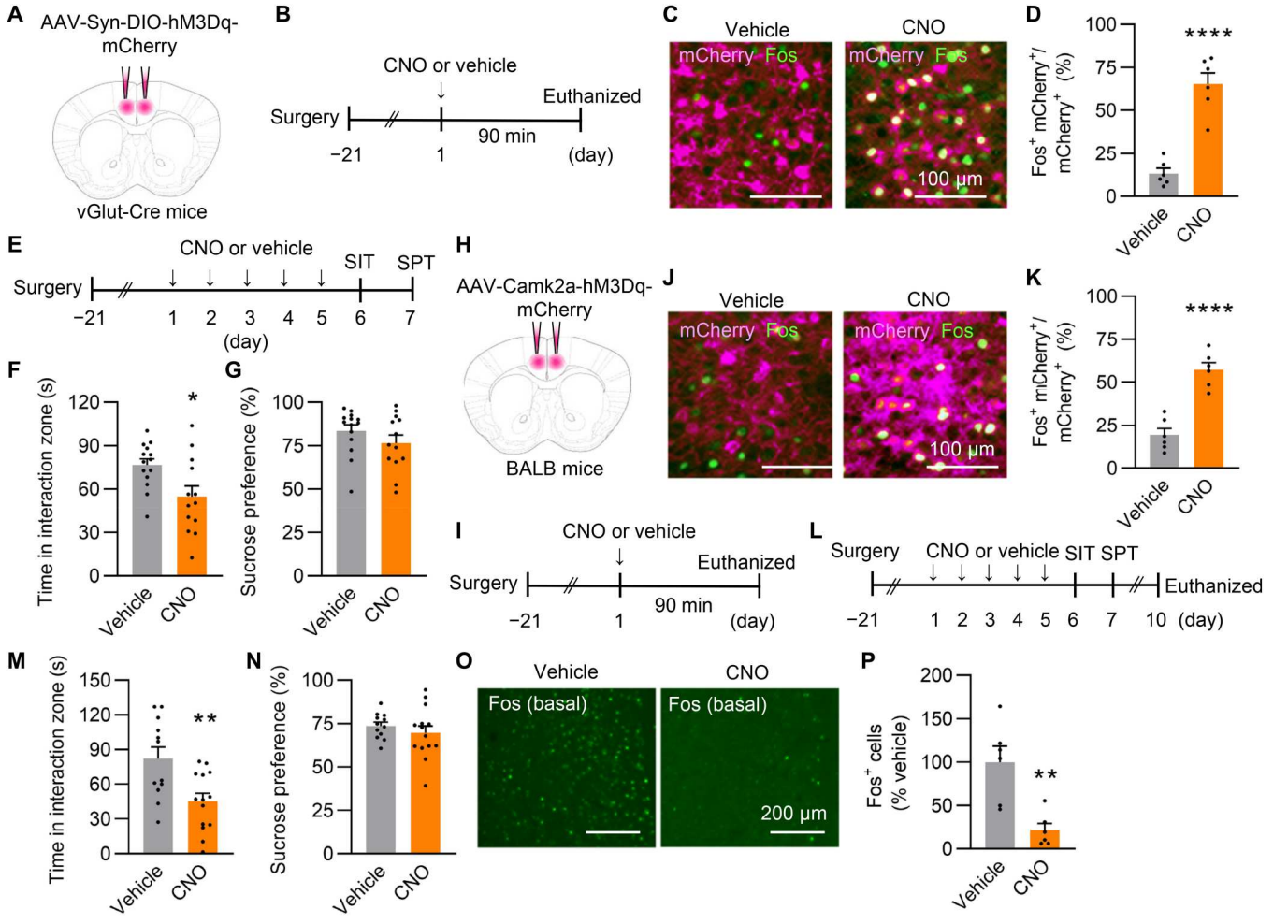

Fig. 6. Activation of Gq-GPCR signaling in ACC glutamatergic neurons leads to social interaction deficit. (**A**) AAV microinjection into the ACC. (**B**) The experimental design for hM3Dq-DREADD validation. (**C**) Immunohistochemical staining showing Fos expression 90 min after the injection of either CNO or vehicle in vGlut-Cre mice expressing hM3Dq-mCherry. Scale bars, 100 μm. (**D**) Fos quantification data (unpaired *t* test, $t_{10} = 7.27$, $P < 0.0001$). $n = 6$ per group. (**E**) The experimental design for behavioral tests. (**F** and **G**) The time spent in the interaction zone of the SIT (F) (unpaired *t* test, $t_{25} = 2.651$, $P < 0.05$) and sucrose preference in the SPT (G) (unpaired *t* test, $t_{25} = 1.219$, $P > 0.05$). $n = 13$ to 14 per group. (**H**) AAV microinjection into the ACC. (**I**) The experimental design for hM3Dq-DREADD validation. (**J**) Immunohistochemical staining showing Fos expression 90 min after the injection of either CNO or vehicle in BALB mice expressing hM3Dq-mCherry. Scale bars, 100 μm. (**K**) Fos quantification data (unpaired *t* test, $t_{10} = 6.702$, $P < 0.0001$). $n = 6$ per group. (**L**) The experimental design for behavioral tests and quantification of baseline Fos expression. (**M** and **N**) The time spent in the interaction zone of the SIT (M) (unpaired *t* test, $t_{24} = 3.135$, $P < 0.01$) and sucrose preference in the SPT (N) (unpaired *t* test, $t_{24} = 0.8495$, $P > 0.05$). $n = 12$ to 14 per group. (**O** and **P**) Representative images (O) and the quantification (P) of baseline Fos levels in the ACC of hM3Dq mice 5 days after the last CNO or vehicle treatment (unpaired *t* test, $t_{10} = 3.909$, $P < 0.01$). $n = 6$ per group. Scale bars, 200 μm. $^*P < 0.05$, $^{**}P < 0.01$, and $^{****}P < 0.0001$. Bar graphs show the means ± SEM.

Chemogenetic activation of Gs-GPCR signaling in ACC glutamatergic neurons during stress drives stress resilience

Our results indicated that activating Gq-GPCR (increased Ca^{2+} signaling) and Gi-GPCR signals (decreased cAMP signaling) reduced social interactions, whereas attenuating Gq-GPCR signals (decreased Ca^{2+} signaling) during SDS drove stress resilience, suggesting that the daily stress-evoked augmentation of the Ca^{2+} and cAMP pathways negatively and positively modulates stress-induced social behaviors. To test this hypothesis, we used rM3Ds-DREADD, which induces neuronal activation by enhancing cAMP-mediated signaling upon CNO treatment (*33*, *36*). The AAV vector containing the excitatory Gs-coupled receptor rM3Ds (AAV-Camk2a-rM3Ds-mCherry) was injected into the ACC of BALB mice (Fig. 8F). We performed Fos immunohistochemistry to validate the efficacy of the Gs-DREADD system and observed increased Fos expression in mCherry-positive glutamatergic neurons 90 min after CNO treatment (Fig. 8, G to I), suggesting the successful activation of Gs-DREADD. Then, the mice were systemically injected with CNO 30 min before SDS exposure during 5 days of smSDS exposure and tested in the SIT and SPT (Fig. 8J). The smSDS-exposed mice treated with CNO spent significantly more time in the interaction zone of the SIT than vehicle-treated stressed mice (Fig. 8K) but exhibited a normal sucrose preference in the SPT (Fig. 8L). We quantified baseline Fos levels (6 days after the termination of the smSDS session) in the ACC of rM3Ds mice treated with CNO during the 5 days of SDS exposure (Fig. 8J) and detected a greater number of Fos-positive cells after treatment with CNO than after treatment with vehicle (Fig. 8, M and N). These results suggest that the activation

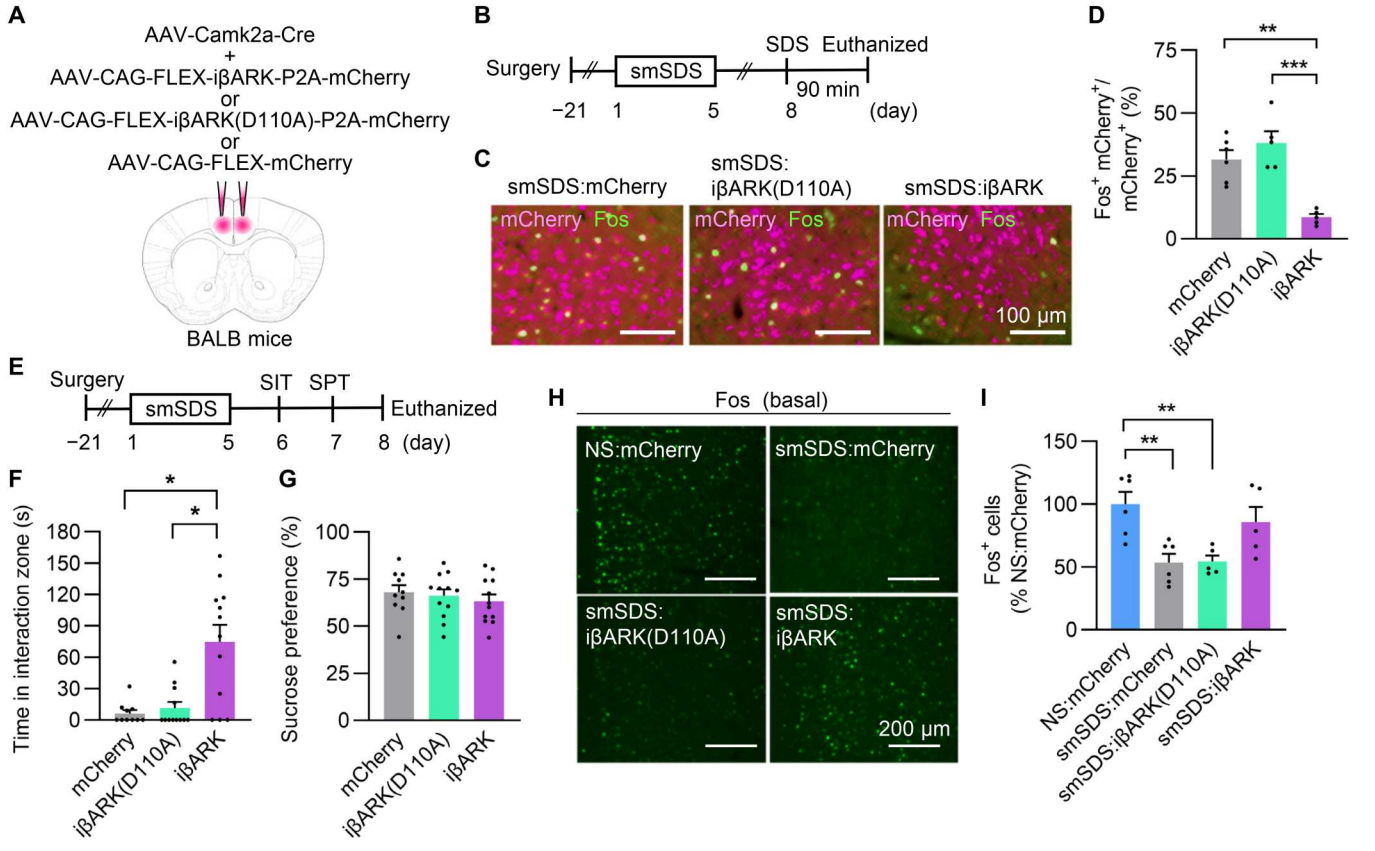

Fig. 7. Inhibition of Gq-GPCR signaling in ACC glutamatergic neurons prevents stress-induced social interaction deficit. (**A**) AAV microinjection into the ACC. (**B**) The experimental design for iβARK validation in BALB mice. (**C**) Immunohistochemical staining showing SDS-evoked Fos induction and mCherry expression in stressed BALB mice injected with either AAV-CAG-FLEX-mCherry, AAV-CAG-FLEX-iβARK-P2A-mCherry, or AAV-CAG-FLEX-iβARK (D110A)-P2A-mCherry. Mice were euthanized 90 min after the sixth SDS exposure. Scale bars, 100 μm. (**D**) Quantification of the Fos immunostaining data shown in (C) [one-way ANOVA, $F_{2,13} = 2.191$, $P < 0.0001$; post hoc test, mCherry versus iβARK, $P < 0.01$, iβARK(D110A) versus iβARK, $P < 0.001$]. $n = 5$ to 6 per group. (**E**) The experimental design for behavioral tests and quantification of baseline Fos levels. (**F** and **G**) The time spent in the interaction zone of the SIT (F) [Kruskal-Wallis, $P < 0.01$, mCherry versus iβARK (D110A), $P < 0.05$, mCherry versus iβARK, $P < 0.05$] and sucrose preference in the SPT (G) (Kruskal-Wallis, $P > 0.05$). $n = 10$ to 12 per group. (**H**) Immunohistochemical staining showing baseline Fos and mCherry expression (72 hours after the 5 days of smSDS) in stressed or nonstressed BALB mice injected with either AAV-CAG-FLEX-mCherry, AAV-CAG-FLEX-iβARK-P2A-mCherry, or AAV-CAG-FLEX-iβARK (D110A)-P2A-mCherry. Scale bars, 200 μm. (**I**) Quantification of baseline Fos expression shown in (H) [one-way ANOVA, $F_{3,18} = 1.796$, $P < 0.01$; post hoc test, NS:mCherry versus smSDS:mCherry, $P < 0.01$, NS:mCherry versus smSDS: iβARK(D110A), $P < 0.01$]. $n = 5$ to 6 per group. *$P < 0.05$, **$P < 0.01$, and ***$P < 0.001$. Bar graphs show the means ± SEM.

of cAMP signaling during smSDS prevents the reduction in baseline Fos levels and drives stress resilience.

Modulation of ACC GABAergic neuronal activity controls the behavioral response to stress

The γ-aminobutyric acid (GABA)–mediated inhibition of pyramidal neuron activity results from the GABA type A receptor–dependent suppression of Ca^{2+} influx through synaptic calcium channels and *N*-methyl-D-aspartate (NMDA) receptors and from the GABA type B receptor–dependent inhibition of cAMP signaling by stimulating Gi-GPCR (*37*–*40*). We therefore investigated whether the suppression of Ca^{2+} influx and cAMP signaling in ACC glutamatergic neurons via GABAergic neuronal activation would affect stress-induced depression-related behaviors. We injected AAVs expressing excitatory hM3Dq-mCherry or mCherry as a control into the ACC of vGat-Cre mice (Fig. 9A) and validated hM3Dq-DREADD function in vGat-Cre mice (Fig. 9B). Immunohistochemistry revealed greater Fos induction in mCherry-positive GABAergic neurons 90 min after treatment with CNO (Fig. 9, C and D) but reduced expression in non-GABAergic cells (Fig. 9E), suggesting the successful activation of GABAergic neurons and subsequent inhibition of non-GABAergic cells. Then, mice were treated with CNO for five consecutive days, and their behaviors were assessed in the SIT and SPT (Fig. 9F). We found that hM3Dq mice treated with CNO spent significantly less time in the interaction zone (Fig. 9G) but spent a normal amount of time in the corner zones (Fig. 9H) in the SIT. We did not observe any significant alterations in the SPT after CNO treatment (Fig. 9I). Therefore, the chemogenetic activation of ACC GABAergic neurons increases the stress vulnerability of social behaviors.

Last, we investigated the effects of GABAergic neuron inhibition on chronic SDS (CSDS)-induced behaviors. We injected AAVs expressing the inhibitory hM4Di-mCherry into the ACC of vGat-Cre mice (Fig. 10A) and validated hM4Di-DREADD by measuring Fos expression 90 min after CNO treatment (Fig. 10B). Immunohistochemistry revealed that CNO treatment increased Fos expression in

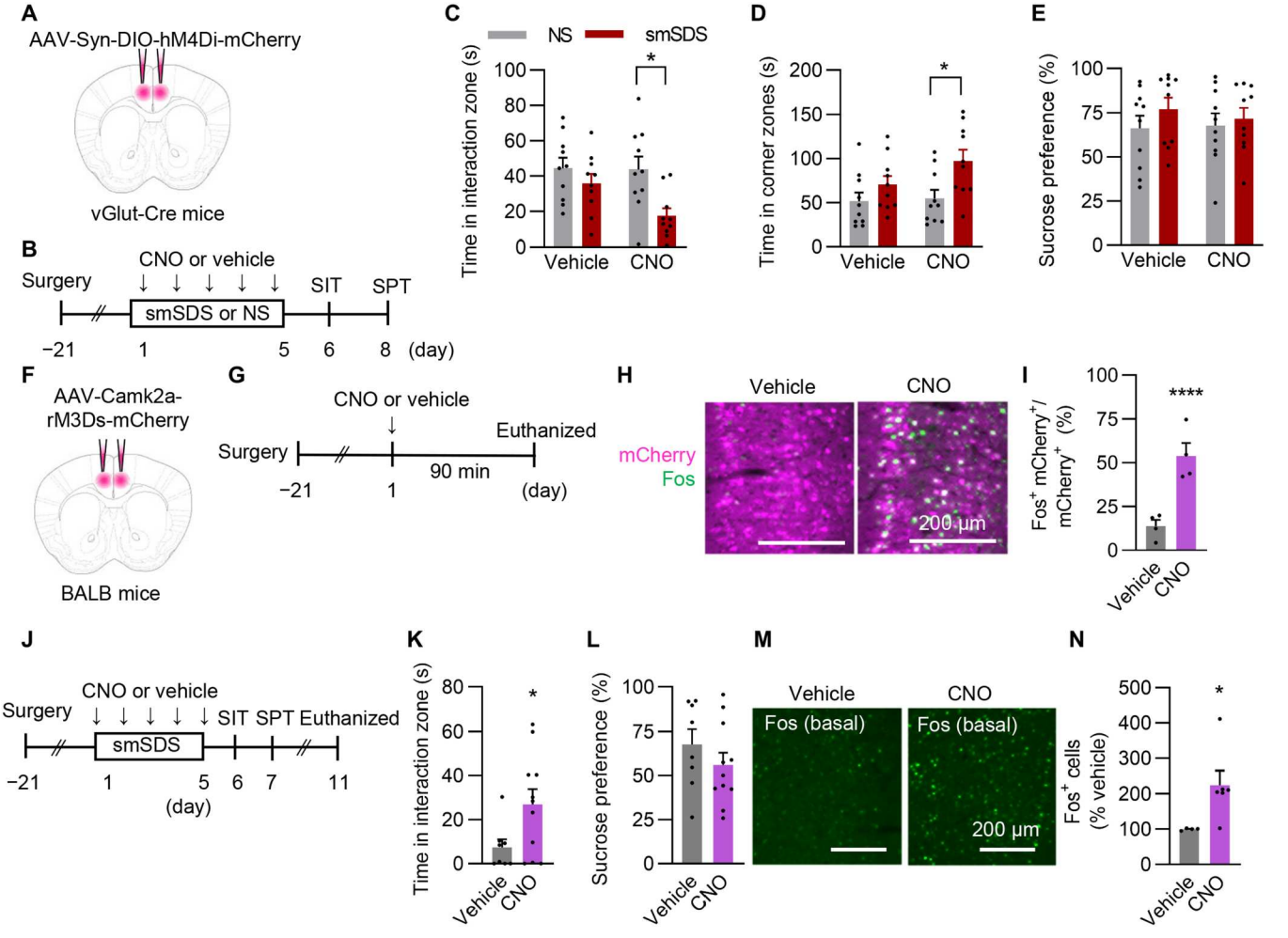

Fig. 8. Effects of chemogenetic modulation of cAMP signaling in ACC glutamatergic neurons during stress on social interaction performance. (**A**) AAV microinjection into the ACC. (**B**) The experimental design for behavioral tests. (**C** to **E**) The time spent in the interaction zone (C) (two-way ANOVA, stress, $F_{1,36} = 9.042$, $P < 0.01$; post hoc test, CNO-NS versus CNO-smSDS, $P < 0.05$) and the time spent in the corner zones (D) (two-way ANOVA, stress, $F_{1,36} = 8.583$, $P < 0.01$; post hoc test, CNO-NS versus CNO-smSDS, $P < 0.05$) of the SIT and sucrose preference in the SPT (E). $n = 10$ per group. (**F**) AAV microinjection into the ACC. (**G**) The experimental design for rM3Ds-DREADD validation in BALB mice. (**H**) Immunohistochemical staining showing Fos and rM3Ds-mCherry expression 90 min after the injection of either CNO or vehicle in BALB mice injected with AAV-Camk2a-rM3Ds-mCherry. Scale bars, 200 μm. (**I**) Fos quantification (unpaired t test, $t_{12} = 6.27$, $P < 0.0001$). $n = 4$ per group. (**J**) The experimental design for behavioral tests and quantification of baseline Fos expression. (**K** and **L**) The time spent in the interaction zone (K) (Welch's test, $t_{14.73} = 2.495$, $P < 0.05$) of the SIT and sucrose preference in the SPT (L) (unpaired t test, $t_{17} = 1.059$, $P > 0.05$). $n = 8$ to 11 per group. (**M** and **N**) Representative images (M) and quantification (N) of baseline Fos levels in the ACC of rM3Ds mice subjected to repeated CNO or vehicle treatment during SDS 6 days after the 5-day smSDS session (unpaired t test, $t_8 = 2.421$, $P < 0.05$). $n = 4$ to 6 per group. Scale bars, 200 μm. ****$P < 0.0001$ and *$P < 0.05$. Bar graphs show the means ± SEM.

the ACC (Fig. 10, C and D) and that this increase in Fos expression was detected in Ca2+/calmodulin-dependent protein kinase II α (CaMKIIα)-positive excitatory neurons (Fig. 10, E and F), indicating successful activation of glutamatergic neurons via the inhibition of GABAergic neurons. We next subjected mice to 10 days of CSDS and tested them in the SIT to identify susceptible mice, which were defined by a social interaction ratio less than 1.0, as previously reported (*20*). The following day, susceptible mice were administered CNO or vehicle once, and 30 min later, the SIT was performed to observe a rapid antidepressant-like effect. The next day, susceptible mice were treated with CNO or vehicle for four consecutive days, and the SIT was performed again to observe the effect of repeated inhibition of ACC GABAergic neurons on CSDS-induced social interaction behaviors (Fig. 10G). We found that the social interaction ratio of CSDS-susceptible mice was significantly increased by either acute or repeated CNO treatment, whereas this increase in the social interaction ratio was not observed in vehicle-treated susceptible mice (Fig. 10, H and I). These data indicated that chemogenetic inhibition of ACC GABAergic neurons leads to antidepressant-like behaviors.

DISCUSSION

In this study, we revealed the molecular and cellular mechanisms underlying repeated stress-induced behavioral changes using a GxE animal model of stress susceptibility and resilience. There are three major findings. First, we performed brain-wide Fos mapping of stress-susceptible mice and found that ACC

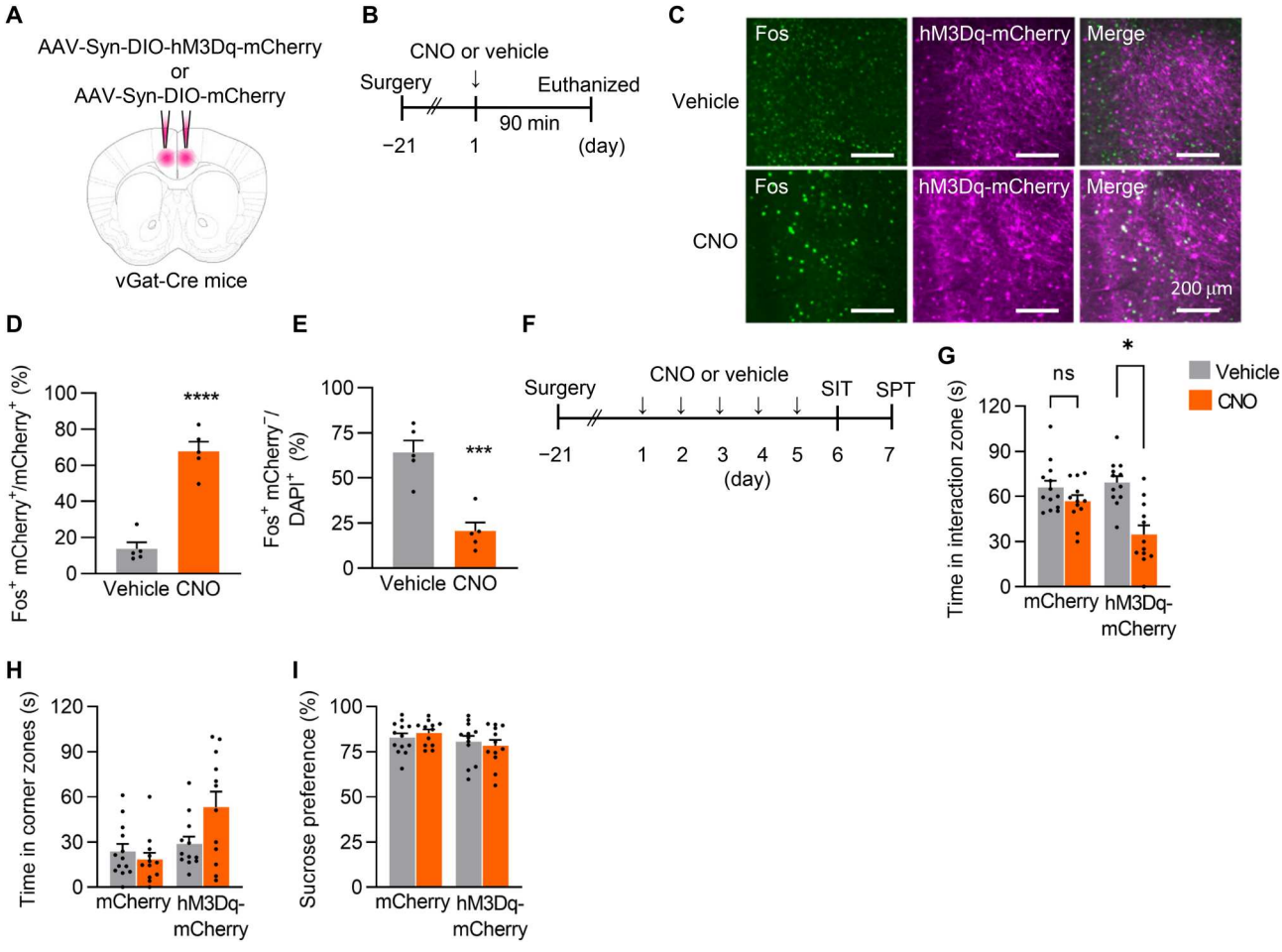

Fig. 9. Chemogenetic activation of ACC GABAergic neurons induces social interaction deficit. (**A**) AAV microinjection into the ACC. (**B**) The experimental design for hM3Dq-DREADD validation in vGat-Cre mice. (**C**) Immunohistochemical staining showing Fos and hM3Dq-mCherry expression 90 min after the injection of either CNO or vehicle in vGat-Cre mice microinjected with AAV-Syn-DIO-hM3Dq-mCherry. Scale bars, 200 μm. (**D** and **E**) Fos quantification in mCherry-positive GABAergic neurons (D) (unpaired *t* test, $t_8 = 8.285$, $P < 0.0001$) and DAPI-positive and mCherry-negative neurons (E) (unpaired *t* test, $t_8 = 5.282$, $P < 0.001$) from the immunostaining data shown in (C). $n = 5$ per group. (**F**) The experimental design for behavioral assays. (**G** to **I**) The time spent in the interaction zone (G) (two-way ANOVA, AAV × drug interaction, $F_{1,45} = 6.92$, $P < 0.05$; post hoc test, hM3Dq-vehicle versus hM3Dq-CNO, $P < 0.05$) and the time spent in the corner zones (H) of the SIT and sucrose preference in the SPT (I). $n = 12$ to 13 per group. *$P < 0.05$, ***$P < 0.001$, and ****$P < 0.0001$. Bar graphs show the means ± SEM.

glutamatergic neurons are necessary for controlling social behaviors under stressful challenges (Figs. 1 to 3). Second, our findings have translational relevance because we observed a reduction in *c-fos* expression in the ACC of patients with MDD, providing human evidence linking Fos dysfunction in the ACC to MDD (Fig. 4). Functionally, we observed that Fos knockdown induced social interaction deficits in B6 mice following smSDS exposure, suggesting important roles of Fos function in the ACC in stress-induced social behaviors (Fig. 5). Third, chemogenetic techniques revealed the roles of calcium and cAMP signals during stress in the habituation process and behavioral response to repeated stress exposure. Repeated increases in Gq-GPCR–mediated calcium signaling and Gs-GPCR-mediated cAMP signaling attenuated and normalized basal Fos levels in the ACC, respectively, contributing to stress-susceptible and stress-resilient behaviors (Figs. 6 to 8). In addition, Gi-GPCR–mediated inhibition of ACC GABAergic neuronal activity ameliorated stress-induced social interaction deficits, suggesting that GABA-mediated disinhibition of ACC glutamatergic neurons exerts antidepressant-like effects (Figs. 9 and 10).

The adult brain is thought to have a high degree of plasticity and flexibility, which is necessary for functional adaptation to environmental changes. Acute stress-induced neural activation is involved in adaptive responses to cope with stressful events (*41*–*43*). In addition, repeated homotypic stressor-induced desensitization of neural activity leads to stress habituation, whereas repeated stressor-induced sensitization of neural activity (lack of stress habituation) is associated with increased depression-like and anxiety behaviors (*8*, *11*, *44*). We found that smSDS-resilient B6 mice exhibited increased Fos expression in the ACC after the first exposure to an unfamiliar aggressor mouse, and this response was decreased by repeated SDS exposure, suggesting the induction of the stress habituation process in this strain. In contrast to B6 mice, ACC neurons of stress-susceptible BALB mice did not respond to the first social stimuli, and ACC neuronal activity was exaggerated and sensitized by the 5 days of smSDS session, suggesting that both the adaptive

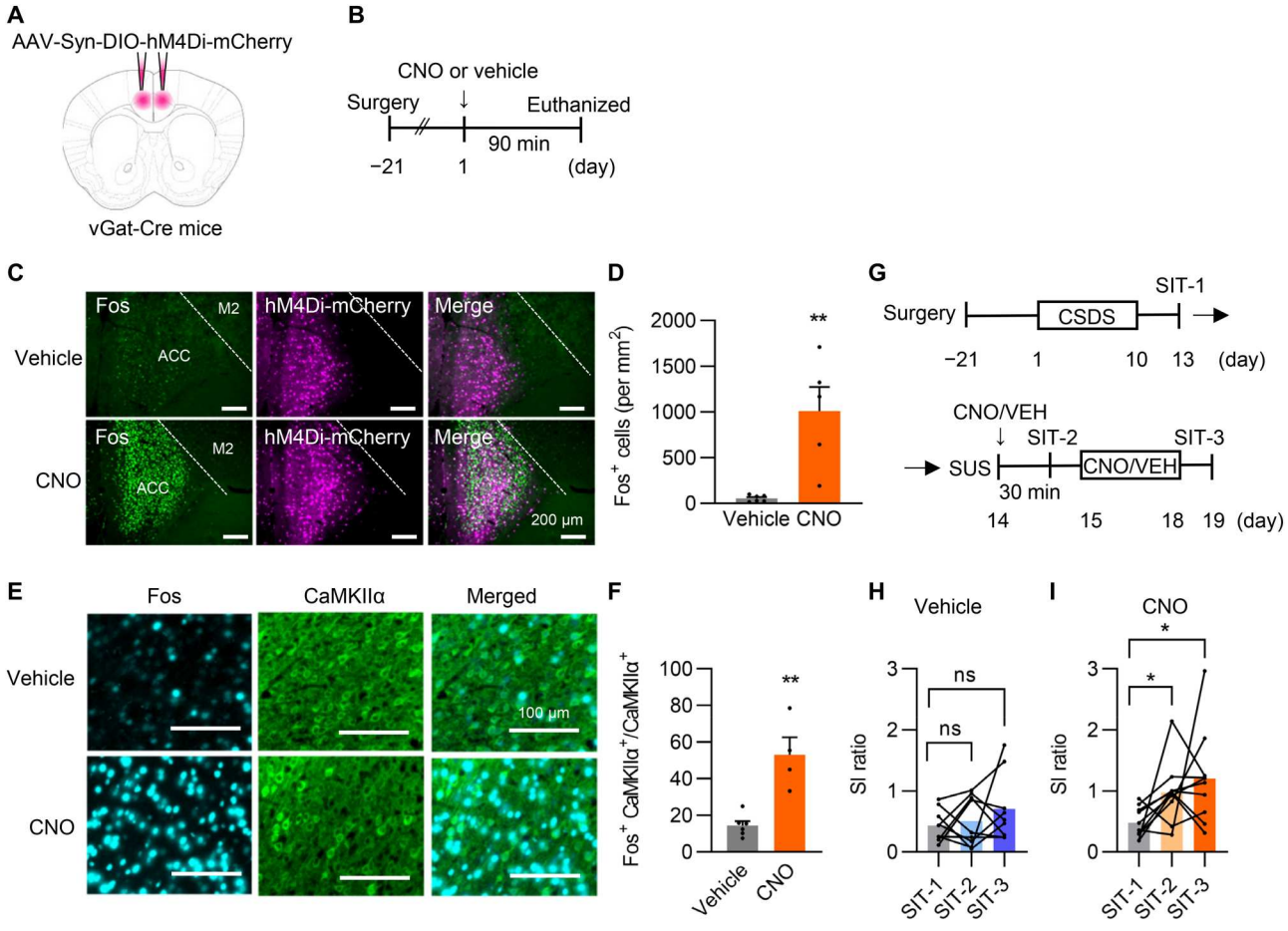

Fig. 10. Chemogenetic inhibition of ACC GABAergic neurons ameliorates stress-induced social interaction deficit. (**A**) AAV microinjection into the ACC. (**B**) The experimental design for hM4Di-DREADD validation in vGat-Cre mice. (**C**) Immunohistochemical staining showing Fos and hM4Di-mCherry expression 90 min after the injection of either CNO or vehicle in vGat-Cre mice microinjected with AAV-Syn-DIO-hM4Di-mCherry. Scale bars, 200 μm. (**D**) Fos quantification in the ACC (unpaired *t* test, $t_9 = 3.967$, $P < 0.01$). $n = 5$ to 6 per group. (**E**) Immunohistochemical staining showing Fos and CaMKIIα expression after the injection of either CNO or vehicle in vGat-Cre mice injected with AAV-Syn-DIO-hM4Di-mCherry. Scale bars, 100 μm. (**F**) Fos quantification in CaMKIIα-positive neurons (E) (unpaired *t* test, $t_8 = 4.714$, $P < 0.01$). $n = 5$ to 6 per group. (**G**) The experimental design for behavioral assays. (**H** and **I**) Social interaction (SI) ratio of hM4Di mice administered vehicle (H) (paired *t* test, SIT-1 versus SIT-2, $t_{8,} = 0.4389$, $P > 0.05$; SIT-1 versus SIT-3, $t_{8,} = 1.38$, $P > 0.05$) and CNO (I) in the SIT (paired *t* test, SIT-1 versus SIT-2, $t_{9,} = 2.509$, $P < 0.05$; SIT-1 versus SIT-3, $t_{9,} = 2.64$, $P < 0.05$). $n = 9$ to 10 per group. *$P < 0.05$ and **$P < 0.01$. Bar graphs show the means ± SEM.

response and stress habituation are deficient in this strain. Overall, BALB mice could be a useful animal model for stress maladaptation and thus allow us to investigate the mechanisms of susceptibility and resilience to stressful stimuli in brain function and behavior.

The mPFC, which includes the prelimbic cortex, infralimbic cortex, and ACC, plays a well-characterized role in social behavior (*24*, *45*, *46*) and is increasingly considered a key node in the neural circuitry that mediates mood and anxiety (*47*, *48*). Here, we used the caspase-mediated ablation of ACC glutamatergic neurons and observed stress vulnerability induced by the ablation of ACC glutamatergic neurons in the B6 strain. In contrast, the BALB strain exhibited reduced social interactions and an increased immobility time following AAC neuron ablation alone. Because the BALB strain is known as a more anxious strain than the B6 strain (*49*), the innate anxious state of BALB strain may act as a stressful situation that confers increased depression-related behaviors. In addition to the ablation experiment, we observed that the modulation of ACC function by DREADDs and iβARK influenced only social interaction behaviors but not sucrose preference. In addition, focal knockdown of Fos within the ACC led to reduced social interactions but did not induce an anhedonic state. As RNA-seq revealed 290 DEGs in stressed BALB mice and we selected only one gene for knockdown, other molecules might be involved in regulating the stress-induced anhedonic state.

The Diagnostic and Statistical Manual of Mental Disorders Fifth edition (DSM-V) lists several core symptoms present in patients with major depression and requires the presence of at least five of nine symptoms (*1*), indicating that patients with major depression show a highly diverse set of combination of symptoms (*50*). Anhedonia is one of the core symptoms of major depression, and two main types of anhedonia have been identified, i.e., physical anhedonia such as eating, touching, or sex, and social anhedonia, such as an overall disinterest in social contact or a lack of pleasure in social engagement (*51*, *52*). Here, we provide evidence for the role of ACC glutamatergic neurons in stress-induced social interaction deficits, but not in sucrose preference. Although we have not clearly

determined whether the reduced social interaction following stress exposure in animals corresponds to social anhedonia in humans, earlier studies reported that a social interaction deficit is an apparent hallmark of depression-related behaviors in animals subjected to chronic SDS (*44*, *53*). Nevertheless, our data suggest a distinct role for ACC glutamatergic neurons in regulating stress-induced social behaviors and sucrose preference. As the different behavioral phenotypes elicited by chronic stress may involve discrete brain areas and circuits (*21*, *54*, *55*), future examinations are required for an in-depth analysis of the mechanisms underlying a subset of stress-induced depression-related behaviors.

In this study, we provide evidence suggesting the important roles of manipulating intracellular signaling cascades rather than simply manipulating neural activity in stress adaptation and behavioral regulation. Our findings complement previous evidence suggesting that chronic activation of cAMP signaling positively modulates brain function and stress-induced behavioral regulation (*36*, *56*–*58*). In contrast to cAMP signaling, our data indicate that the repeated activation of calcium signaling via stimulation of Gq-GPCR in the ACC negatively regulates the stress adaptation process and confers social interaction deficits. However, we and other researchers have reported that the activation of calcium signaling via synaptic calcium-permeable AMPARs: α-amino-3-hydroxy-5-methyl-4-isoxazolepropionic acid receptors (AMPARs) (i.e., GluA1) are associated with stress resilience and antidepressant-like behaviors (*13*, *59*–*63*). The reason for this contradiction is unclear, but because Gq-GPCR activation promotes Ca^{2+} release from the endoplasmic reticulum (ER), one possibility is that the source of Ca^{2+} may be important for downstream molecular and cellular processes and subsequent behavioral adaptations to stress. More specifically, we speculate that repeated Ca^{2+} influx via synaptic receptors/channels is associated with stress resilience, whereas increased Ca^{2+} release from the ER as a result of Gq-GPCR activation conversely leads to stress susceptibility. Critically, we found that the activation and inhibition of the Gq-GPCR pathway negatively and positively regulated stress-induced social interaction behavior, respectively. In addition, the activation of ACC GABAergic neurons, which presumably inhibit action potential-evoked Ca^{2+} signals through synaptic calcium channels and NMDA receptors (*37*, *39*) and thereby inhibits glutamatergic neurons, leads to social interaction deficits. A previous report has shown that biased peptides that prevent Gq-mediated calcium signaling but induce an enhanced synaptic AMPAR-mediated calcium response contribute to antidepressant actions (*64*). Moreover, the expression levels of RyR1 and RyR3, which are channels present on the membrane of the ER, were significantly increased in a mouse model of depression (*65*), and the blockade and the inhibition of the RyRs induced antidepressant-like behaviors (*66*). Thus, the activation of calcium signaling as a consequence of Ca^{2+} influx from synaptic receptors/channels and the Ca^{2+} release from the ER during stress may have opposite roles in modulating the behavioral response to repeated stress.

In summary, our study indicates that repeated stress-induced sensitization of ACC neurons reduces baseline Fos levels and eventually induces social interaction deficits in BALB mice, whereas repeated stress-induced desensitization of ACC neurons maintains baseline Fos levels and drives stress resilience in B6 mice. Mechanistically, the effects of GPCR-mediated calcium and cAMP signaling on *c-fos* expression may be the underlying mechanisms required for cellular and behavioral maladaptation and adaptation to stress. This study not only characterizes a preclinical model representing the nuanced effects of GxE interactions but also provides insight into the multilevel neuronal processes (i.e., gene expression, intracellular signaling, and neuronal activity) underlying stress-induced regulation of social behaviors. These findings could provide insight into the pathophysiology of stress-related disorders, as well as into the development of medications that target these pathways to prevent stress-induced dysfunction.

MATERIALS AND METHODS

General experimental design

No statistical methods were used to predetermine sample sizes. The sample sizes in this study were determined on the basis of the experience of previous studies and the previous literature using similar experimental paradigms. Some data were excluded from the statistical analyses for mice with missed AAV injections. The number of biological or technical replicates for each experimental group is listed in the corresponding figure legends. Independent animals were used as biological replicates in all experiments. Samples from each animal were evaluated in technical duplicate for qPCR. RNA-seq data were not replicated in independent experiments due to resource restrictions, but the data were validated with qPCR. For the quantification of immunofluorescence images, at least three images were analyzed per animal. Behavioral results were replicated in multiple mice. All attempts at replication were successful. All mice were randomly assigned to different groups. Animals were allocated into experimental groups by sex, age, etc. The investigators were not blinded during data acquisition or analysis due to the conditions of the experiments. However, the parameters and processes in each experiment were consistently applied for all groups.

Animals

Adult male C57BL/6J, BALB/c, and retired breeder CD1 mice were purchased from Charles River Japan. The vGluT2-IRES::Cre and vGat-IRES::Cre mice were obtained from JAX (vGlut-Cre mice; JAX stock #016963, vGat-Cre mice; JAX stock #016962). All data reported in this study were collected with male mice. All mice were housed under a 12-hour light/12-hour dark cycle (8:00 to 20:00 light) with food and water available ad libitum. All animal studies and experimental procedures were approved by the Animal Care and Use Committees of Kyoto University.

Social defeat stress

SDS was performed for 10 days (CSDS), as previously reported (*20*, *44*). Retired male breeder CD1 mice were used as aggressors and housed in the social defeat cage. B6 mice were placed in the cage of the CD1 aggressor for a period of 10 min/day. After this defeat session, the test mice were separated from the aggressor resident by placing the Plexiglas divider perforated with small holes to allow sensory contact over a 24-hour period. To assess stress susceptibility, we used an abbreviated subthreshold SDS, referred to as smSDS (*13*). In this paradigm, B6 and BALB mice were subjected to defeat stress for a period of 5 min for five consecutive days, while the other procedures were the same as in the CSDS condition described above.

Behavioral tests

All behavioral experiments were performed between 9:00 and 16:00.

Social interaction test

The SIT was performed as previously reported (*13*). All subjects were individually placed in a 42 cm by 42 cm arena with an empty wire mesh cage (10 cm by 6.5 cm) for 3 min, followed by 3 min in the presence of an unfamiliar CD1 mouse (for smSDS experiments) or an unfamiliar BALB or B6 mouse (for non-smSDS experiments; Figs. 3H, 6, E and L, and 9F) enclosed in the wire cage in the arena. Time spent in the area surrounding the wire cage (interaction zone, 24 cm by 14 cm) and in the corner zones (9 cm by 9 cm) opposite to the interaction zone was measured automatically with an ANY-maze tracking system (Stoelting). The results are shown as the time spent in the target and/or corner zones or as the interaction ratio, which was calculated by dividing the time spent in the target zone in the presence of a social target by the time spent in the target zone in the absence of the social target. A susceptible individual was defined by a ratio less than 1 (*20*).

Sucrose preference test

On the day before the test, the bedding in the cage and food chow were replaced, and the animals were deprived of water. On the day of the test, mice were exposed to one bottle containing tap water and one bottle containing 1.5% sucrose solution for 4 hours. The bottle side and animal group tests were counterbalanced among chambers to prevent possible effects of a side preference on drinking behavior. The preference for the sucrose solution was expressed as the percentage of sucrose intake relative to the total intake.

Tail suspension test

Mice were individually suspended by their tails with a plastic clip 45 cm above the floor in three-walled rectangular compartments. Mouse movements were video recorded, and the duration of immobility (all four limbs stopped struggling or only slight body movement occurred) was manually measured for 6 min.

Immunohistochemistry

Mice were deeply anesthetized with avertin and then transcardially perfused with phosphate-buffered saline (PBS) followed by a 4% paraformaldehyde (PFA) solution (4°C). The brains were removed and postfixed with 4% PFA in phosphate buffer (PB) overnight, followed by cryoprotection with 30% sucrose in PB. Twenty-micrometer-thick coronal sections were generated with a cryostat (Leica). Antibodies against Fos (1:500 or 1:1000; Cell Signaling, #2250), CaMKIIα (1:500; Abcam, ab22609), NeuN (1:1000; Millipore, MAB377), and hemagglutinin (HA; 1:1000, Merck, #11867423001) were used. Secondary antibodies were conjugated with Alexa Fluor 488, Alexa Fluor 555, or Alexa Fluor 647 (1:1000; Life Technologies). Sections were mounted on slides and coverslipped with Vectashield (Vector Laboratories). Images were acquired using a fluorescence microscope (Keyence BZ-X800) and processed with BZ-X800 analyzer software (Keyence). For Fos quantification, three to four brain slices per mouse were collected, and images were background subtracted and then thresholded using the Max Entropy function with ImageJ [National Institutes of Health (NIH)]. All images were processed and analyzed using ImageJ software (NIH). Images were thresholded using the Max Entropy algorithm. The number of Fos-positive cells was estimated using the "Analyze Particle" function. A colocalization analysis was performed to determine the number of mCherry-positive or CaMKIIα-positive cells coexpressing Fos using CellProfiler software (Broad Institute) (*67*).

TUNEL staining

Apoptotic neurons induced by taCasp3-TEVp were visualized using a TUNEL assay kit (In Situ Cell Death Detection, Fluorescein) according to the manufacturer′s instructions. Briefly, sections were fixed with 4% PFA for 20 min, rinsed with PBS for 30 min, and permeabilized with 0.1% sodium citrate buffer containing 0.1% Triton X-100 for 2 min. Then, the sections were stained using the TUNEL staining kit and subsequently counterstained with 4′,6-diamidino-2-phenylindole (DAPI). Images were acquired using a fluorescence microscope (Keyence BZ-X800).

AAV-mediated gene transfer

The AAV vector plasmids pAAV-EF1a-FLEX-taCasp3-TEVp (a gift from N. Shah and J. Wells, Addgene plasmid #45580), pAAV-Camk2a-Cre (a gift from J. M. Wilson, Addgene plasmid #105558), pAAV-Syn-DIO-hM3Dq-mCherry (a gift from B. Roth, Addgene plasmid #44361), pAAV-Syn-DIO-hM4Di-mCherry (a gift from B. Roth, Addgene plasmid #44362), pAAV-Camk2a-hM3Dq-mCherry (a gift from B. Roth, Addgene plasmid #50467), pAAV-Syn-DIO-mCherry (a gift from B. Roth, Addgene plasmid #50459), pAAV-Syn-DIO-rM3Ds-mCherry (a gift from B. Roth, Addgene plasmid #50458), pAAV-CAG-FLEX-iβARK-P2A-mCherry (Addgene plasmid #117693), and pAAV-CAG-FLEX-iβARK(D110A)-P2A-mCherry (Addgene plasmid #117694) were obtained from Addgene. The AAV vector plasmids pAAV-U6-sgFos-Camk2a(0.4 kb)-SaCas9-HA, pAAV-U6-sgControl-Camk2a(0.4 kb)-SaCas9-HA, pAAV-Camk2a-rM3Ds-mCherry, AAV5-EF1a-FLEX-nls-tdTomato (denoted as AAV5-EF1a-FLEX-tdTomato), and pAAV-CAG-FLEX-mCherry were constructed and obtained from VectorBuilder Japan (Kanagawa, Japan). The genomic titer of each virus was determined using qPCR. AAV5-EF1a-FLEX-taCasp3-TEVp [titer: 1.2×10^{13} vector genome (vg)/ml], AAV5-EF1a-FLEX-tdTomato (titer: 1.5×10^{13} vg/ml), and AAV5-CAG-FLEX-mCherry (titer: 3.5×10^{13} vg/ml) were packaged and purified in the Laboratory of Vector Biolabs (Malvern, PA). AAV8-U6-sgFos-Camk2a-SaCas9-HA (titer: 7.4×10^{13} vg/ml), AAV8-U6-sgControl-Camk2a-SaCas9-HA (titer: 8.2×10^{13} vg/ml), and AAV8-Camk2a-rM3Ds-mCherry (titer: 7.7×10^{13} vg/ml) were packaged and purified in the Laboratory of VectorBuilder. AAV5-Camk2a-Cre (titer: 1.5×10^{13} vg/ml, Addgene #105558-AAV5), AAV5-Syn-DIO-hM3Dq-mCherry (titer: 2.7×10^{13} vg/ml, Addgene #44361-AAV5), AAV8-Camk2a-hM3Dq-mCherry (titer: 2.8×10^{13} vg/ml, Addgene #50476-AAV8), AAV5-Syn-DIO-hM4Di-mCherry (titer: 2.5×10^{13} vg/ml, Addgene #44362-AAV5), and AAV5-Syn-DIO-mCherry (titer: 2.3×10^{13} vg/ml, Addgene #50459-AAV5) were obtained from Addgene. AAV5-CAG-FLEX-iβARK-P2A-mCherry (titer: 1.0×10^{13} vg/ml) and AAV5-CAG-FLEX-iβARK(D110A)-P2A-mCherry (titer: 1.0×10^{13} vg/ml) were packaged and purified in our laboratory.

For the AAV injection, mice were anesthetized with isoflurane (induction dose of ~2.0% and maintenance dose of ~1.5%) and placed in a stereotaxic frame (David Kopf Instruments). AAV vectors were dissolved in physiological saline and injected bilaterally into the ACC (150 nl of the AAV solution, anteroposterior (AP), +0.98 mm; mediolateral (ML), ±0.3 mm; dorsoventral (DV), −1.9 mm from the bregma) with a glass micropipette and an air pressure injection system (BJ-110, BEX, Japan). The needle was slowly withdrawn after 5 min. Mice were allowed to recover for at least 3 weeks for maximum transgene induction. To validate viral spread in the

mice used in this study, mice were euthanized after behavior testing, and we confirmed AAV-driven transgene expression (i.e., mCherry, tdTomato, and HA) or apoptosis (TUNEL).

Drug treatment

CNO (Toronto Research Chemicals, Toronto, Canada) was dissolved in saline and delivered intraperitoneally at a dose of 10 ml/kg. The applied doses were 1.0 and 5.0 mg/kg for chemogenetic activation (hM3Dq and rM3Ds) and inhibition (hM4Di) experiments, respectively.

Tissue dissection

Mice were anesthetized with isoflurane, and whole brains were quickly sliced into 1-mm coronal sections (bregma, 1.38 to 0.38 mm) using a brain matrix (Bio Research Center Co. Ltd.) and then further dissected to isolate the ACC region (Cg1 and Cg2) under a stereomicroscope. ACC tissue was harvested using a 1-mm-diameter tissue punch (Stoelting) on freshly cut 1-mm-thick coronal sections. Tissues were then snap-frozen in liquid nitrogen and stored at −80°C.

RNA extraction

Total RNA was extracted with TRIzol reagent (Thermo Fisher Scientific) and Direct-zol RNA Miniprep Plus (Zymo Research) according to the manufacturers' instructions. We calculated the RNA concentration using a spectrophotometer (NanoDrop, Thermo Fisher Scientific) based on the A260/A280 ratio, which was 1.93 to 2.01 for all RNA preparations. Samples for RNA-seq had RNA Integrity Number (RIN) values > 8.5 (BioAnalyzer, Agilent).

RNA sequencing

RNA-seq libraries were generated using the SMART-Seq v4 Ultra Low Input RNA Kit (Takara Bio) and the TruSeq RNA Sample Prep Kit v2 (Illumina) according to the manufacturer's instructions. The quality of the libraries was assessed using an Agilent 2200 TapeStation High Sensitivity D1000 instrument (Agilent Technologies, Santa Clara, CA). Libraries were sequenced on a NovaSeq 6000 (Illumina) with a configuration of 2 × 100 bp (Macrogen). Then, sequencing adaptors, low-quality reads, and bases were trimmed with the Trimmomatic-0.38 tool (*68*). The sequence reads were aligned to the reference mouse genome (mm10) using HISAT2 version 2.1.0 (*69*). After read mapping, StringTie (*70*) was used for transcript assembly, and the expression profile was calculated for each sample and transcript/gene as the read count. The iDEP platform (version 0.94) (*71*) was used to process the count data, and DEGs were extracted using DESeq2 (*72*). DEG sets were selected when genes were 1.2-fold up/down-regulated and had a Benjamini-Hochberg adjusted P value (false discovery rate P) < 0.15 for comparisons between two groups (*42*, *73*). The list of DEGs is shown in data S1. Gene ontology term enrichment analysis, transcriptional regulatory network analysis (TRRUST), and PPI network analysis were conducted using the Metascape platform (*31*). The raw sequencing data were deposited in Gene Expression Omnibus (GEO; GSE207854). The RNA-seq data for the subgenual ACC from patients with MDD (N = 51) and control subjects (N = 55) were reported previously (*30*), and the processed data presented in their paper were used to identify overlapping DEGs between BALB mice subjected to smSDS and human MDD (Fig. 4B).

Quantitative polymerase chain reaction

qPCR was performed as previously described (*13*, *74*). One hundred nanograms of total RNA was used for cDNA synthesis using the QuantiTect Reverse Transcription Kit (Qiagen). qPCR amplification was performed using a StepOnePlus Real-Time PCR System (Thermo Fisher Scientific) with SYBR green FAST Master Mix (Thermo Fisher Scientific) according to the manufacturer's protocol. The sequences of the primers used in this study are shown in table S1. All measurements were performed in duplicate. The *Gapdh* expression level was used to normalize the relative expression levels of each target mRNA.

Statistical analyses

GraphPad Prism (version 9.0; GraphPad Software Inc.) was used to analyze the data. If applicable, multiple unpaired t tests, two-tailed paired or unpaired t tests, Welch's test, the Kruskal-Wallis test, or one- or two-way analysis of variance (ANOVA) followed by Tukey's multiple comparisons test, Bonferroni's correction, or Dunn's test was used. In all cases, differences were considered significant at $P < 0.05$. All data are presented as the means ± SEM.

Supplementary Materials

This PDF file includes:
Figs. S1 to S3
Table S1
Legends for data S1

Other Supplementary Material for this manuscript includes the following:
Data file S1

View/request a protocol for this paper from *Bio-protocol*.

REFERENCES AND NOTES

1. American Psychiatric Association, *The Diagnostic and Statistical Manual of Mental Disorders, Fifth Edition*, (American Psychiatric Association, 2013).
2. P. F. Sullivan, M. C. Neale, K. S. Kendler, Genetic epidemiology of major depression: Review and meta-analysis. *Am. J. Psychiatry* **157**, 1552–1562 (2000).
3. S. J. Russo, E. J. Nestler, The brain reward circuitry in mood disorders. *Nat. Rev. Neurosci.* **14**, 609–625 (2013).
4. S. M. Southwick, D. S. Charney, The science of resilience: Implications for the prevention and treatment of depression. *Science* **338**, 79–82 (2012).
5. S. Uchida, H. Yamagata, T. Seki, Y. Watanabe, Epigenetic mechanisms of major depression: Targeting neuronal plasticity. *Psychiatry Clin. Neurosci.* **72**, 212–227 (2018).
6. V. Krishnan, E. J. Nestler, The molecular neurobiology of depression. *Nature* **455**, 894–902 (2008).
7. A. Kawatake-Kuno, T. Murai, S. Uchida, The molecular basis of depression: Implications of sex-related differences in epigenetic regulation. *Front. Mol. Neurosci.* **14**, 708004 (2021).
8. J. P. Herman, Neural control of chronic stress adaptation. *Front. Behav. Neurosci.* **7**, 61 (2013).
9. E. R. de Kloet, M. Joels, F. Holsboer, Stress and the brain: From adaptation to disease. *Nat. Rev. Neurosci.* **6**, 463–475 (2005).
10. B. S. McEwen, N. P. Bowles, J. D. Gray, M. N. Hill, R. G. Hunter, I. N. Karatsoreos, C. Nasca, Mechanisms of stress in the brain. *Nat. Neurosci.* **18**, 1353–1363 (2015).
11. S. Uchida, A. Nishida, K. Hara, T. Kamemoto, M. Suetsugi, M. Fujimoto, T. Watanuki, Y. Wakabayashi, K. Otsuki, B. S. McEwen, Y. Watanabe, Characterization of the vulnerability to repeated stress in Fischer 344 rats: Possible involvement of microRNA-mediated down-regulation of the glucocorticoid receptor. *Eur. J. Neurosci.* **27**, 2250–2261 (2008).

12. L. J. Sittig, P. Carbonetto, K. A. Engel, K. S. Krauss, C. M. Barrios-Camacho, A. A. Palmer, Genetic background limits generalizability of genotype-phenotype relationships. *Neuron* **91**, 1253–1259 (2016).
13. Y. Sakai, H. Li, H. Inaba, Y. Funayama, E. Ishimori, A. Kawatake-Kuno, H. Yamagata, T. Seki, T. Hobara, S. Nakagawa, Y. Watanabe, S. Tomita, T. Murai, S. Uchida, Gene-environment interactions mediate stress susceptibility and resilience through the CaMKIIbeta/TARP-gamma-8/AMPAR pathway. *iScience* **24**, 102504 (2021).
14. S. Uchida, K. Hara, A. Kobayashi, K. Otsuki, H. Yamagata, T. Hobara, T. Suzuki, N. Miyata, Y. Watanabe, Epigenetic status of Gdnf in the ventral striatum determines susceptibility and adaptation to daily stressful events. *Neuron* **69**, 359–372 (2011).
15. D. D. Francis, K. Szegda, G. Campbell, W. D. Martin, T. R. Insel, Epigenetic sources of behavioral differences in mice. *Nat. Neurosci.* **6**, 445–446 (2003).
16. K. Mozhui, R.-M. Karlsson, T. L. Kash, J. Ihne, M. Norcross, S. Patel, M. R. Farrell, E. E. Hill, C. Graybeal, K. P. Martin, M. Camp, P. J. Fitzgerald, D. C. Ciobanu, R. Sprengel, M. Mishina, C. L. Wellman, D. G. Winder, R. W. Williams, A. Holmes, Strain differences in stress responsivity are associated with divergent amygdala gene expression and glutamate-mediated neuronal excitability. *J. Neurosci.* **30**, 5357–5367 (2010).
17. T. Funayama, H. Li, E. Ishimori, A. Kawatake-Kuno, H. Inaba, H. Yamagata, T. Seki, S. Nakagawa, Y. Watanabe, T. Murai, N. Oishi, S. Uchida, Antidepressant response and stress resilience are promoted by CART peptides in GABAergic neurons of the anterior cingulate cortex. *Biol. Psychiatry Glob. Open Sci.* **3**, 87–98 (2023).
18. S. C. Dulawa, K. A. Holick, B. Gundersen, R. Hen, Effects of chronic fluoxetine in animal models of anxiety and depression. *Neuropsychopharmacology* **29**, 1321–1330 (2004).
19. X. Zhang, J.-M. Beaulieu, T. D. Sotnikova, R. R. Gainetdinov, M. G. Caron, Tryptophan hydroxylase-2 controls brain serotonin synthesis. *Science* **305**, 217 (2004).
20. V. Krishnan, M.-H. Han, D. L. Graham, O. Berton, W. Renthal, S. J. Russo, Q. Laplant, A. Graham, M. Lutter, D. C. Lagace, S. Ghose, R. Reister, P. Tannous, T. A. Green, R. L. Neve, S. Chakravarty, A. Kumar, A. J. Eisch, D. W. Self, F. S. Lee, C. A. Tamminga, D. C. Cooper, H. K. Gershenfeld, E. J. Nestler, Molecular adaptations underlying susceptibility and resistance to social defeat in brain reward regions. *Cell* **131**, 391–404 (2007).
21. I. Cerniauskas, J. Winterer, J. W. de Jong, D. Lukacsovich, H. Yang, F. Khan, J. R. Peck, S. K. Obayashi, V. Lilascharoen, B. K. Lim, C. Foldy, S. Lammel, Chronic stress induces activity, synaptic, and transcriptional remodeling of the lateral habenula associated with deficits in motivated behaviors. *Neuron* **104**, 899–915.e8 (2019).
22. M. Girotti, T. W. W. Pace, R. I. Gaylord, B. A. Rubin, J. P. Herman, R. L. Spencer, Habituation to repeated restraint stress is associated with lack of stress-induced c-fos expression in primary sensory processing areas of the rat brain. *Neuroscience* **138**, 1067–1081 (2006).
23. E.-L. Yap, N. L. Pettit, C. P. Davis, M. A. Nagy, D. A. Harmin, E. Golden, O. Dagliyan, C. Lin, S. Rudolph, N. Sharma, E. C. Griffith, C. D. Harvey, M. E. Greenberg, Bidirectional perisomatic inhibitory plasticity of a *Fos* neuronal network. *Nature* **590**, 115–121 (2021).
24. Y. E. Wu, W. Hong, Neural basis of prosocial behavior. *Trends Neurosci.* **45**, 749–762 (2022).
25. W. C. Drevets, J. Savitz, M. Trimble, The subgenual anterior cingulate cortex in mood disorders. *CNS Spectr.* **13**, 663–681 (2008).
26. P. W. Frankland, C. O'Brien, M. Ohno, A. Kirkwood, A. J. Silva, Alpha-CaMKII-dependent plasticity in the cortex is required for permanent memory. *Nature* **411**, 309–313 (2001).
27. A. Goto, A. Bota, K. Miya, J. Wang, S. Tsukamoto, X. Jiang, D. Hirai, M. Murayama, T. Matsuda, T. J. McHugh, T. Nagai, Y. Hayashi, Stepwise synaptic plasticity events drive the early phase of memory consolidation. *Science* **374**, 857–863 (2021).
28. H. Tost, F. A. Champagne, A. Meyer-Lindenberg, Environmental influence in the brain, human welfare and mental health. *Nat. Neurosci.* **18**, 1421–1431 (2015).
29. C. F. Yang, M. C. Chiang, D. C. Gray, M. Prabhakaran, M. Alvarado, S. A. Juntti, E. K. Unger, J. A. Wells, N. M. Shah, Sexually dimorphic neurons in the ventromedial hypothalamus govern mating in both sexes and aggression in males. *Cell* **153**, 896–909 (2013).
30. N. Akula, S. Marenco, K. Johnson, N. Feng, K. Zhu, A. Schulmann, W. Corona, X. Jiang, J. Cross, B. England, A. Nathan, S. Detera-Wadleigh, Q. Xu, P. K. Auluck, K. An, R. Kramer, J. Apud, B. T. Harris, C. Harker Rhodes, B. K. Lipska, F. J. McMahon, Deep transcriptome sequencing of subgenual anterior cingulate cortex reveals cross-diagnostic and diagnosis-specific RNA expression changes in major psychiatric disorders. *Neuropsychopharmacology* **46**, 1364–1372 (2021).
31. Y. Zhou, B. Zhou, L. Pache, M. Chang, A. H. Khodabakhshi, O. Tanaseichuk, C. Benner, S. K. Chanda, Metascape provides a biologist-oriented resource for the analysis of systems-level datasets. *Nat. Commun.* **10**, 1523 (2019).
32. F. A. Ran, L. Cong, W. X. Yan, D. A. Scott, J. S. Gootenberg, A. J. Kriz, B. Zetsche, O. Shalem, X. Wu, K. S. Makarova, E. V. Koonin, P. A. Sharp, F. Zhang, *In vivo* genome editing using *Staphylococcus aureus* Cas9. *Nature* **520**, 186–191 (2015).
33. B. L. Roth, DREADDs for Neuroscientists. *Neuron* **89**, 683–694 (2016).
34. G. M. Alexander, S. C. Rogan, A. I. Abbas, B. N. Armbruster, Y. Pei, J. A. Allen, R. J. Nonneman, J. Hartmann, S. S. Moy, M. A. Nicolelis, J. O. McNamara, B. L. Roth, Remote control of neuronal activity in transgenic mice expressing evolved G protein-coupled receptors. *Neuron* **63**, 27–39 (2009).
35. J. Nagai, A. Bellafard, Z. Qu, X. Yu, M. Ollivier, M. R. Gangwani, B. Diaz-Castro, G. Coppola, S. M. Schumacher, P. Golshani, V. Gradinaru, B. S. Khakh, Specific and behaviorally consequential astrocyte G_q GPCR signaling attenuation in vivo with iβARK. *Neuron* **109**, 2256–2274.e9 (2021).
36. K. A. Lyman, Y. Han, C. Zhou, I. Renteria, G.-L. Besing, J. E. Kurz, D. M. Chetkovich, Hippocampal cAMP regulates HCN channel function on two time scales with differential effects on animal behavior. *Sci. Transl. Med.* **13**, eabl4580 (2021).
37. C. Q. Chiu, G. Lur, T. M. Morse, N. T. Carnevale, G. C. R. Ellis-Davies, M. J. Higley, Compartmentalization of GABAergic inhibition by dendritic spines. *Science* **340**, 759–762 (2013).
38. M. Korczak, P. Kurowski, A. Lesniak, A. Gronbladh, A. Filipowska, M. Bujalska-Zadrozny, $GABA_B$ receptor intracellular signaling: Novel pathways for depressive disorder treatment? *Eur. J. Pharmacol.* **885**, 173531 (2020).
39. J. J. Marlin, A. G. Carter, GABA-A receptor inhibition of local calcium signaling in spines and dendrites. *J. Neurosci.* **34**, 15898–15911 (2014).
40. M. Farrant, Z. Nusser, Variations on an inhibitory theme: Phasic and tonic activation of GABA(A) receptors. *Nat. Rev. Neurosci.* **6**, 215–229 (2005).
41. B. S. McEwen, H. Akil, Revisiting the stress concept: Implications for affective disorders. *J. Neurosci.* **40**, 12–21 (2020).
42. C. Nasca, B. Bigio, D. Zelli, P. de Angelis, T. Lau, M. Okamoto, H. Soya, J. Ni, L. Brichta, P. Greengard, R. L. Neve, F. S. Lee, B. S. McEwen, Role of the astroglial glutamate exchanger xCT in ventral hippocampus in resilience to stress. *Neuron* **96**, 402–413.e5 (2017).
43. N. Grissom, S. Bhatnagar, Habituation to repeated stress: Get used to it. *Neurobiol. Learn. Mem.* **92**, 215–224 (2009).
44. O. Berton, C. A. McClung, R. J. Dileone, V. Krishnan, W. Renthal, S. J. Russo, D. Graham, N. M. Tsankova, C. A. Bolanos, M. Rios, L. M. Monteggia, D. W. Self, E. J. Nestler, Essential role of BDNF in the mesolimbic dopamine pathway in social defeat stress. *Science* **311**, 864–868 (2006).
45. K. Yamamuro, L. K. Bicks, M. B. Leventhal, D. Kato, S. Im, M. E. Flanigan, Y. Garkun, K. J. Norman, K. Caro, M. Sadahiro, K. Kullander, S. Akbarian, S. J. Russo, H. Morishita, A prefrontal-paraventricular thalamus circuit requires juvenile social experience to regulate adult sociability in mice. *Nat. Neurosci.* **23**, 1240–1252 (2020).
46. L. K. Bicks, H. Koike, S. Akbarian, H. Morishita, Prefrontal cortex and social cognition in mouse and man. *Front. Psychol.* **6**, 1805 (2015).
47. J. E. Ploski, V. A. Vaidya, The neurocircuitry of posttraumatic stress disorder and major depression: Insights into overlapping and distinct circuit dysfunction-A tribute to Ron Duman. *Biol. Psychiatry* **90**, 109–117 (2021).
48. D. A. Pizzagalli, A. C. Roberts, Prefrontal cortex and depression. *Neuropsychopharmacology* **47**, 225–246 (2022).
49. I. Hovatta, R. S. Tennant, R. Helton, R. A. Marr, O. Singer, J. M. Redwine, J. A. Ellison, E. E. Schadt, I. M. Verma, D. J. Lockhart, C. Barlow, Glyoxalase 1 and glutathione reductase 1 regulate anxiety in mice. *Nature* **438**, 662–666 (2005).
50. P. Willner, J. Scheel-Kruger, C. Belzung, The neurobiology of depression and antidepressant action. *Neurosci. Biobehav. Rev.* **37**, 2331–2371 (2013).
51. E. Barkus, J. C. Badcock, A transdiagnostic perspective on social anhedonia. *Front. Psych.* **10**, 216 (2019).
52. L. J. Chapman, J. P. Chapman, M. L. Raulin, Scales for physical and social anhedonia. *J. Abnorm. Psychol.* **85**, 374–382 (1976).
53. N. M. Tsankova, O. Berton, W. Renthal, A. Kumar, R. L. Neve, E. J. Nestler, Sustained hippocampal chromatin regulation in a mouse model of depression and antidepressant action. *Nat. Neurosci.* **9**, 519–525 (2006).
54. D. Knowland, V. Lilascharoen, C. P. Pacia, S. Shin, E. H.-J. Wang, B. K. Lim, Distinct ventral pallidal neural populations mediate separate symptoms of depression. *Cell* **170**, 284–297.e18 (2017).
55. Z. Zheng, C. Guo, M. Li, L. Yang, P. Liu, X. Zhang, Y. Liu, X. Guo, S. Cao, Y. Dong, C. Zhang, M. Chen, J. Xu, H. Hu, Y. Cui, Hypothalamus-habenula potentiation encodes chronic stress experience and drives depression onset. *Neuron* **110**, 1400–1415.e6 (2022).
56. Y. Dwivedi, A. C. Mondal, P. K. Shukla, H. S. Rizavi, J. Lyons, Altered protein kinase a in brain of learned helpless rats: Effects of acute and repeated stress. *Biol. Psychiatry* **56**, 30–40 (2004).
57. Y. Zhang, W. Lu, Z. Wang, R. Zhang, Y. Xie, S. Guo, L. Jiao, Y. Hong, Z. Di, G. Wang, J. Aa, Reduced neuronal cAMP in the nucleus accumbens damages blood-brain barrier integrity and promotes stress vulnerability. *Biol. Psychiatry* **87**, 526–537 (2020).
58. F. Plattner, K. Hayashi, A. Hernandez, D. R. Benavides, T. C. Tassin, C. Tan, J. Day, M. W. Fina, E. Y. Yuen, Z. Yan, M. S. Goldberg, A. C. Nairn, P. Greengard, E. J. Nestler, R. Taussig, A. Nishi, M. D. Houslay, J. A. Bibb, The role of ventral striatal cAMP signaling in stress-induced behaviors. *Nat. Neurosci.* **18**, 1094–1100 (2015).

59. A. Kawatake-Kuno, T. Murai, S. Uchida, A multiscale view of the mechanisms underlying ketamine's antidepressant effects: An update on neuronal calcium signaling. *Front. Behav. Neurosci.* **15**, 749180 (2021).
60. N. Li, B. Lee, R.-J. Liu, M. Banasr, J. M. Dwyer, M. Iwata, X.-Y. Li, G. Aghajanian, R. S. Duman, mTOR-dependent synapse formation underlies the rapid antidepressant effects of NMDA antagonists. *Science* **329**, 959–964 (2010).
61. R. S. Duman, R. Shinohara, M. V. Fogaca, B. Hare, Neurobiology of rapid-acting antidepressants: Convergent effects on GluA1-synaptic function. *Mol. Psychiatry* **24**, 1816–1832 (2019).
62. A. J. Kallarackal, M. D. Kvarta, E. Cammarata, L. Jaberi, X. Cai, A. M. Bailey, S. M. Thompson, Chronic stress induces a selective decrease in AMPA receptor-mediated synaptic excitation at hippocampal temporoammonic-CA1 synapses. *J. Neurosci.* **33**, 15669–15674 (2013).
63. X. Cai, A. J. Kallarackal, M. D. Kvarta, S. Goluskin, K. Gaylor, A. M. Bailey, H.-K. Lee, R. L. Huganir, S. M. Thompson, Local potentiation of excitatory synapses by serotonin and its alteration in rodent models of depression. *Nat. Neurosci.* **16**, 464–472 (2013).
64. A. Holz, F. Mulsch, M. K. Schwarz, M. Hollmann, M. D. Dobrossy, V. A. Coenen, M. Bartos, C. Normann, K. Biber, D. van Calker, T. Serchov, Enhanced mGlu5 signaling in excitatory neurons promotes rapid antidepressant effects via AMPA receptor activation. *Neuron* **104**, 338–352.e7 (2019).
65. E. Nakamura-Maruyama, R. Kai, N. Himi, N. Okabe, K. Narita, T. Miyazaki, S. Aoki, O. Miyamoto, Ryanodine receptors are involved in the improvement of depression-like behaviors through electroconvulsive shock in stressed mice. *Brain Stimul.* **14**, 36–47 (2021).
66. N. Galeotti, E. Vivoli, A. Bartolini, C. Ghelardini, A gene-specific cerebral types 1, 2, and 3 RyR protein knockdown induces an antidepressant-like effect in mice. *J. Neurochem.* **106**, 2385–2394 (2008).
67. D. R. Stirling, M. J. Swain-Bowden, A. M. Lucas, A. E. Carpenter, B. A. Cimini, A. Goodman, CellProfiler 4: Improvements in speed, utility and usability. *BMC Bioinformatics* **22**, 433 (2021).
68. A. M. Bolger, M. Lohse, B. Usadel, Trimmomatic: A flexible trimmer for Illumina sequence data. *Bioinformatics* **30**, 2114–2120 (2014).
69. D. Kim, J. M. Paggi, C. Park, C. Bennett, S. L. Salzberg, Graph-based genome alignment and genotyping with HISAT2 and HISAT-genotype. *Nat. Biotechnol.* **37**, 907–915 (2019).
70. M. Pertea, G. M. Pertea, C. M. Antonescu, T.-C. Chang, J. T. Mendell, S. L. Salzberg, StringTie enables improved reconstruction of a transcriptome from RNA-seq reads. *Nat. Biotechnol.* **33**, 290–295 (2015).
71. S. X. Ge, E. W. Son, R. Yao, iDEP: An integrated web application for differential expression and pathway analysis of RNA-Seq data. *BMC Bioinformatics* **19**, 534 (2018).
72. M. I. Love, W. Huber, S. Anders, Moderated estimation of fold change and dispersion for RNA-seq data with DESeq2. *Genome Biol.* **15**, 550 (2014).
73. D. M. Walker, A. M. Cunningham, E. J. Nestler, Reply to: Multiple comparisons and inappropriate statistical testing lead to spurious sex differences in gene expression. *Biol. Psychiatry* **91**, e3–e5 (2022).
74. G. Martel, S. Uchida, C. Hevi, I. Chevere-Torres, I. Fuentes, Y. J. Park, H. Hafeez, H. Yamagata, Y. Watanabe, G. P. Shumyatsky, Genetic demonstration of a role for stathmin in adult hippocampal neurogenesis, spinogenesis, and NMDA receptor-dependent memory. *J. Neurosci.* **36**, 1185–1202 (2016).

Acknowledgments: We thank N. Yasuda and E. Ishimori for technical assistance. **Funding:** This work was supported in part by JSPS KAKENHI grant numbers JP22H03532 (to S.U.), JP21H00198 (to S.U.), JP21K19707 (to S.U.), JP21K15711 (to H.L.), JP22K15625 (to K.D.), JP21H00220 (to J.N.), JP21H02588 (to J.N.), JP21H05640 (to J.N.), JP21K07593 (to N.O.), and JP21H02849 (to T.M. and N.O.), and JP21H05173 (To T.M.), by AMED under grant numbers JP22ak0101136 (to S.U.) and JP22dm0307102 (to T.M.), and by Shionogi and Co. Ltd. (to S.U.). **Author contributions:** Conceptualization: H.I. and S.U. Methodology: H.I., A.K-K., H.L., J.N., K.D., and S.U. Validation: H.I., A.K-K., H.L., and S.U. Formal analysis: H.I., N.O., and S.U. Investigation: H.I., A.K-K., H.L., and S.U. Resources: J.N. and K.D. Writing (original draft): H.I. and S.U. Writing (review and editing): H.I., H.L., A. K-K., J.N., N.O., T.M., and S.U. Visualization: H.I., N.O., and S.U. Funding acquisition: H.L., N.O., J.N., T.M., and S.U. Supervision: T.M. **Competing interests:** J.N. is a scientific advisor for Flox Bio Inc. The other authors declare that they have no competing interests. **Data and materials availability:** All data needed to evaluate the conclusions in the paper are present in the paper and/or the Supplementary Materials. The raw RNA-seq data were deposited in GEO (GSE207854) (www.ncbi.nlm.nih.gov/geo/).

Submitted 30 August 2022
Accepted 2 March 2023
Published 5 April 2023
10.1126/sciadv.ade5397

Science Advances

GPCR-mediated calcium and cAMP signaling determines psychosocial stress susceptibility and resiliency

Hiromichi Inaba, Haiyan Li, Ayako Kawatake-Kuno, Ken-ichi Dewa, Jun Nagai, Naoya Oishi, Toshiya Murai, and Shusaku Uchida

Sci. Adv., **9** (14), eade5397.
DOI: 10.1126/sciadv.ade5397